International Journal of Rock Mechanics & Mining Sciences 136 (2020) 104535

Contents lists available at ScienceDirect

International Journal of Rock Mechanics and Mining Sciences

journal homepage: www.elsevier.com/locate/ijrmms

Bentonite homogenisation during the closure of void spaces

J.F. Harrington [a,*], K.A. Daniels [a], A.C. Wiseall [a], P. Sellin [b]

[a] British Geological Survey, Nicker Hill, Keyworth, Nottinghamshire, NG12 5GG, UK
[b] Svensk Kärnbränslehantering AB (SKB), Brahegatan 47, Stockholm, 10240, Sweden

ARTICLE INFO

Keywords:
Radioactive waste disposal
Engineered barriers
Bentonite
Homogenisation
Swelling pressure

ABSTRACT

In a geological repository, the disposal of radioactive waste will result in the creation of engineering voids. Bentonite is commonly proposed as a sealing material as a result of its high swelling capacity. As the bentonite expands, the non-uniform development of porewater pressure and its coupling to total stress within the bentonite, may impair homogenisation. In this study we present results from five laboratory tests performed on sodium- and calcium-based bentonites to examine their swelling potential and capacity to homogenise over extreme bentonite-to-void ratios. Results demonstrate that even under these extreme ratios, the bentonite is able to swell and ultimately fill each void, creating a small swelling pressure. The swelling pressure development is spatially complex and time-consuming, and does not appear to be influenced by friction. Instead, it is characterised by plastic yielding of the clay with 70%–80% of the volume change associated with clay expansion adjacent to the void. This leads to heterogeneity illustrated by the presence of persistent differential stresses and the non-uniform distribution of moisture contents. Increases in the moisture content were measured but did not always correlate with the development of swelling pressure. This disequilibrium of the system is likely a reflection of the test durations and the slow evolution in the rates of change in swelling and porewater pressure beyond 130 days. Given the length of the experimental tests presented here, the time required to achieve full homogenisation of the clay is likely to be many years, if it occurs at all. Gravity segregation was also present in horizontal tests, further impairing clay homogenisation. However, as presented in this paper, it is possible to define functional relationships describing the bentonite swelling potential across engineering voids of differing size. This information will assist in establishing a safety case for bentonite usage in geological radioactive waste disposal.

1. Introduction

Geological disposal of radioactive waste is the favoured option for many nations for the removal and isolation of hazardous material from the biosphere.[1–3] Disposal designs are dependent on the geology available, with nations usually proposing to use a clay backfill material surrounding the waste in either a clay-based[4–6] or crystalline[1,7] host-rock. The clay backfill forms an engineered barrier system (EBS), which is an integral part of the geological disposal concept.[1] In the KBS3 concept, compacted bentonite will be packed around the HLW canisters.[8] Many concepts include the EBS as stacked blocks,[9–12] and this will introduce engineering voids between the bricks, the waste and the EBS, and the EBS and the host rock. The clay backfill must be able to swell to close these void spaces and prevent them acting as high permeability pathways over the repository lifetime (>100,000 years). Bentonite is commonly chosen to be the clay backfill material[13–15] because of its favourable physical and chemical properties including low permeability and high swelling capacity.[16–19] Both sodium (Na) and calcium (Ca) bentonites have been considered for use within Europe,[20–24] although a greater emphasis has been placed on Na-bentonites such as MX80[25] and FEBEX,[26,27] primarily because of its lower cost.[28] Comparing the two, Marcial and co-workers[29] studied the compression characteristics, observing that the Ca-bentonite still had a larger void ratio and suggesting that the reduced compression was related to the larger diameter of the divalent Ca^{2+} cation. Ben Rhaïem and co-authors[30] found that Na-bentonite contained an increased number of smaller pores than the Ca-bentonite, suggesting that the Na-bentonite had a higher hydration and swelling capacity.

Understanding the behaviour of bentonite and its long-term performance is critical for establishing a safety case for its use in the geological disposal of radioactive waste. Many researchers have studied the swelling (or its inverse, the suction) pressures of bentonite under volumetric confinement[31–40] and these tests have shown that

* Corresponding author.
E-mail address: jfha@bgs.ac.uk (J.F. Harrington).

[1] The difference between the maximum and minimum stress within a system.

https://doi.org/10.1016/j.ijrmms.2020.104535
Received 6 May 2020; Received in revised form 13 October 2020; Accepted 20 October 2020

bentonites with higher dry densities exert an increased swelling pressure when hydrated.[5,41–43] In addition, Gray and co-workers[43] found that below a threshold value of dry density, the lateral and vertical swelling pressure were similar, whilst above the threshold, the vertical swelling was larger. Anisotropy between axial and radial swelling pressures was also presented by Saba and co-authors,[44] although they found the anisotropy to be greater at lower dry densities. As bentonite expands upon contact with water, both a non-uniform[45–49] and non-monotonic[50–55] development of porewater and swelling pressure within the bentonite has been observed. The non-uniform evolution of the bentonite's properties as it hydrates may result in persistent material heterogeneities that could adversely affect the long-term performance of the backfill in the repository setting. Differential stress[1] reduces as hydration progresses,[48,49] whilst variations in density, permeability and mechanical properties remain. The continued endurance of these property variations, along with the final degree of homogenisation (i.e. uniformity), is poorly understood.

Repository safety cases require functional reliability over long time periods.[56] To satisfy this, a greater certainty in the description of the long-term behaviour of bentonite, combined with a full understanding of the development and persistence of heterogeneities (e.g. locked in stresses, density variations, persistent interfaces etc.) within the clay, is needed. In addition, the accurate description of key parameters such as the swelling pressure, permeability, strength, and friction coefficients, will all be affected by temporal constraints encountered by the development and distribution of porewater pressure within the buffer.[49] Indeed, such slow time-dependent phenomena associated with wetting, as well as the possibility of these processes being strongly localised, may account for a significant component of the heterogeneity observed in many laboratory- and full-scale experiments.[27,57] To address these knowledge gaps, the results of a series of bespoke laboratory experiments are presented that examine the long-term distribution of swelling pressure within precompacted bentonites. The tests investigated the homogenisation and swelling capacity of a bentonite sample as it swelled into an engineering void, as a function of the initial sample size, bentonite composition and swelling orientation. These experiments provide unique data on the swelling behaviour of bentonite under extreme material-to-void ratios, providing an indication of the amount of material that would be required for void space closure.

2. Experimental method

A constant volume cell with a cylindrical bore was used to volumetrically constrain the samples in each test, mimicking the boundary conditions of the KBS3 disposal concept.[20,48,49] In analogue form, this configuration represented the borehole and unyielding surface of the host-rock wall, which are key features of the repository near-field for the purposes of this homogenisation study. Two different pieces of apparatus were used so that tests could be run simultaneously (Fig. 1), however both set-ups shared the same basic volumetric constraint, with an internal diameter of 60 mm and an internal length of 120 mm (Apparatus 1) or 116 mm (Apparatus 2). Although they had different sensor configurations, the vessels were instrumented with a series of load cells to directly measure the development of total stress at multiple locations around the sample. Apparatus 1 (vertical tests) was fitted with 8 radial and 4 axial pressure cells to provide a detailed picture for the development of total stress around the sample (Fig. 2). Apparatus 2 (horizontal tests) had fewer load cells measuring total stress (3 radial and 2 axial), but was instrumented with 12 radial pore pressure transducers (Fig. 3). The load cells in Apparatus 2 were housed on the outside of the vessel, with a tungsten carbide pushrod running from the internal face of the vessel to the housing on the outside. This configuration allowed the swelling stress of the clay to be translated to the load cell, but due to the indirect nature of the measurement, meant that the data were slightly more prone to hysteresis. Before the apparatuses were calibrated and the samples installed, the tubework was carefully flushed of residual gas with the test fluid (distilled water) through each of the ports in sequence. All sensors were calibrated against laboratory standards in increasing and decreasing increments to allow quantification of hysteresis. A least squares linear regression of the data was then performed and the corrections were applied to each sensor. The pressures quoted in this paper (with the exception of the load cells in Apparatus 2) should be considered accurate to ±15 kPa. In Apparatus 2, because of the nature of the pushrod configuration (Fig. 1), the load cell measurements can only be considered as accurate to ±80 kPa. In this apparatus, the pore pressure ports were fitted with porous plugs to prevent clay material from migrating into the instrumentation holes. After calibration and flushing, the sample was immediately installed to minimise drying and the remaining void space within the apparatus was filled with distilled water.

High precision Teledyne ISCO D-Series 260D syringe pumps were used to apply a fluid pressure to each end of the sample, and then to control or monitor the flow rate into or out of the sample using a single digital control unit. The position of each pump piston was determined by an optically encoded disc graduated in segments equivalent to a change in volume of 16.63 nL. Movement of the pump piston was controlled by a microprocessor which continuously monitors and adjusts the rate of rotation of the encoded disc using a DC-motor connected to the piston assembly via a geared worm drive. This allowed each pump to operate in either constant pressure or continuous flow modes. The volumetric control system for each pump was factory calibrated. Laboratory calibration of the volumetric data was not practical with available laboratory equipment, so the test programme was designed in such a way as to minimise possible pump errors. All of the tests were performed with distilled water as the external pressurising fluid. Once the pressure had been applied, no external hydraulic gradient was thereafter applied to the clay. The flow rates, total stress and pore pressure were all logged at an interval of 2 min using the FieldPoint™ and cRIO logging hardware and the LabVIEW™ data acquisition software (National Instruments Corporation, Austin, TX, USA), providing a detailed time series dataset. To allow comparison, each test was run for a sufficient time to delineate the swelling response (Table 1). Upon completion of testing, the samples were carefully extruded from the apparatus and cut in approximately 10 mm thick samples. These were then weighed, placed in an oven at 105 °C and dried to determine the moisture content.

3. Results

The basic geotechnical properties of the samples are shown in Table 1. Each sample was manufactured to a nominal diameter of 60 mm, with exact measurements given in Table 1. Start lengths were varied to assess their impact on the swelling behaviour of the clay. Following insertion of each sample into the apparatus, the pore pressure was carefully increased in a series of steps to the target value of 4500 kPa; this value was set with the radioactive waste management company Svensk Karnbranslehantering (SKB) as a suitable reference value comparable to the current Swedish repository concept.

3.1. Development of stress

3.1.1. Tests 1, 2 and 3 (vertical tests)

Fig. 4A shows the development of swelling pressure (i.e. difference between measured pressure and externally applied water pressure) within the apparatus as the sample in Test 1 swells. It is clear from the data that the development of pressure is a spatially complex and time consuming process, with significant variance still existing as the test was terminated (at day 100) (Fig. 4B). Given that the rate of pressure change observed during the latter stages of testing is very small, extrapolation of the results suggests that homogenisation of the bentonite would not occur for many years (if at all). However, it is clear that bentonite, under zero hydraulic gradient, is able to swell and

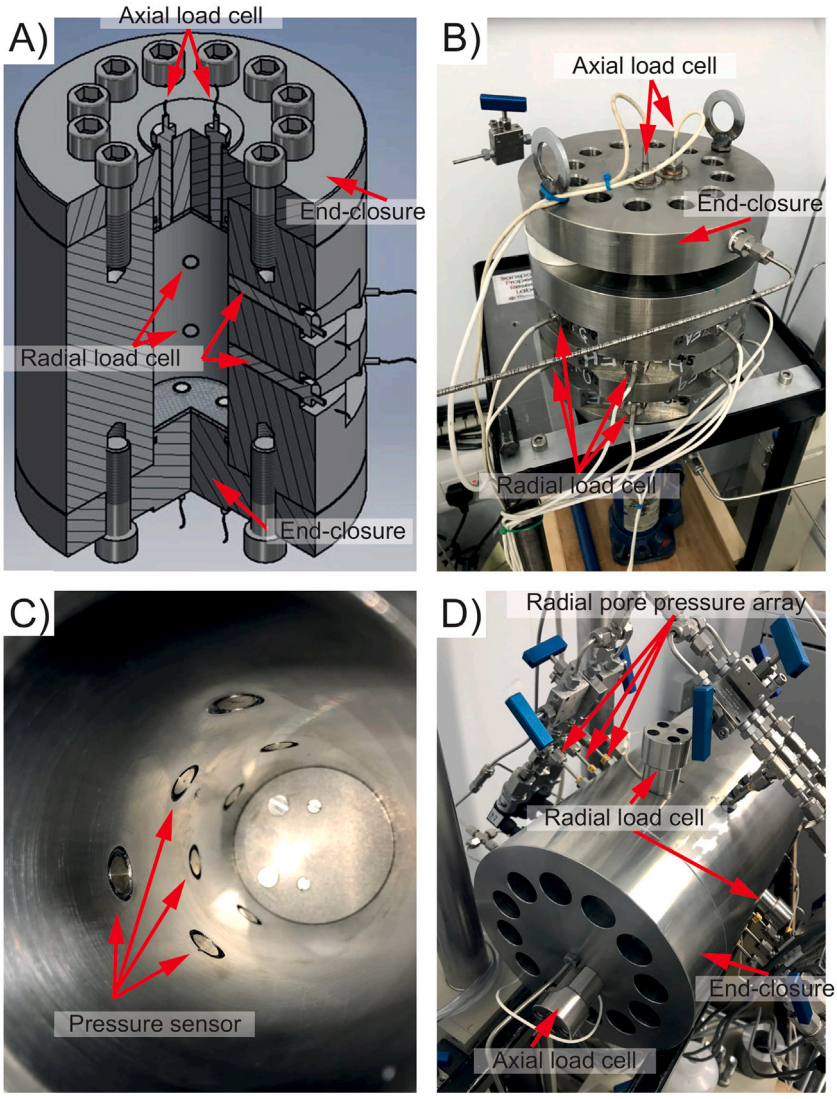

Fig. 1. The apparatuses used for testing. (A–C) Apparatus 1 cut-through schematic and photographs of the outside and inside of the vessel, showing the positions of the axial and radial total stress sensors. (D) Photograph of Apparatus 2 showing locations of the porewater pressure transducers and load cell housings.

Table 1
Basic geotechnical properties of the pre-test material and the starting conditions of the experiments. The samples are assumed to be at 100% saturation, which is a reasonable assumption based on pre-test calibration work. The dry density is a measured value obtained from a test sample made in advance of the testing programme, specifically to obtain the geotechnical properties of the starting material. The test samples were then manufactured using an identical method. The test fluid was distilled water in every test and the porewater pressure was held at 4500 kPa. A testing temperature of 20 ± 1 °C was maintained by an air conditioning system in the laboratory.

Test no.	Sample orientation	Bentonite clay type	Sample length (mm)	Sample diameter (mm)	Void length (mm)	Bulk density (g/cm^3)	Dry density (g/cm^3)	Test duration (days)	Test apparatus
1	Vertical	Sodium (Na), MX80	65.0	59.7	55.0	2.057	1.702	99.75	1
2	Vertical	Sodium (Na), MX80	74.7	59.5	45.3	2.054	1.702	139.22	1
3	Vertical	Sodium (Na), MX80	85.2	59.7	34.8	2.055	1.702	127.00	1
4	Horizontal	Sodium (Na), MX80	65.2	59.7	50.8	2.047	1.702	76.18	2
5	Horizontal	Calcium (Ca)	65.0	59.8	51.0	2.021	Unknown	101.75	2

ultimately fill the start void, creating a small but measurable swelling pressure in the axial sensors above the sample (seen in axial sensors A1 and A2).

The first 10 days of Test 1 show a complex swelling response (Fig. 4C). After the external porewater pressure is applied to the sample, the highest force registered in the clay is at sensor R6, 17 mm below the top of the sample. Significant anisotropy in the swelling response is then observed, with R5 (located in the same plane as R6, Fig. 2) exhibiting a substantially lower pressure (a difference of > 2000 kPa for the first 3 days of testing). Whilst this may simply reflect the availability

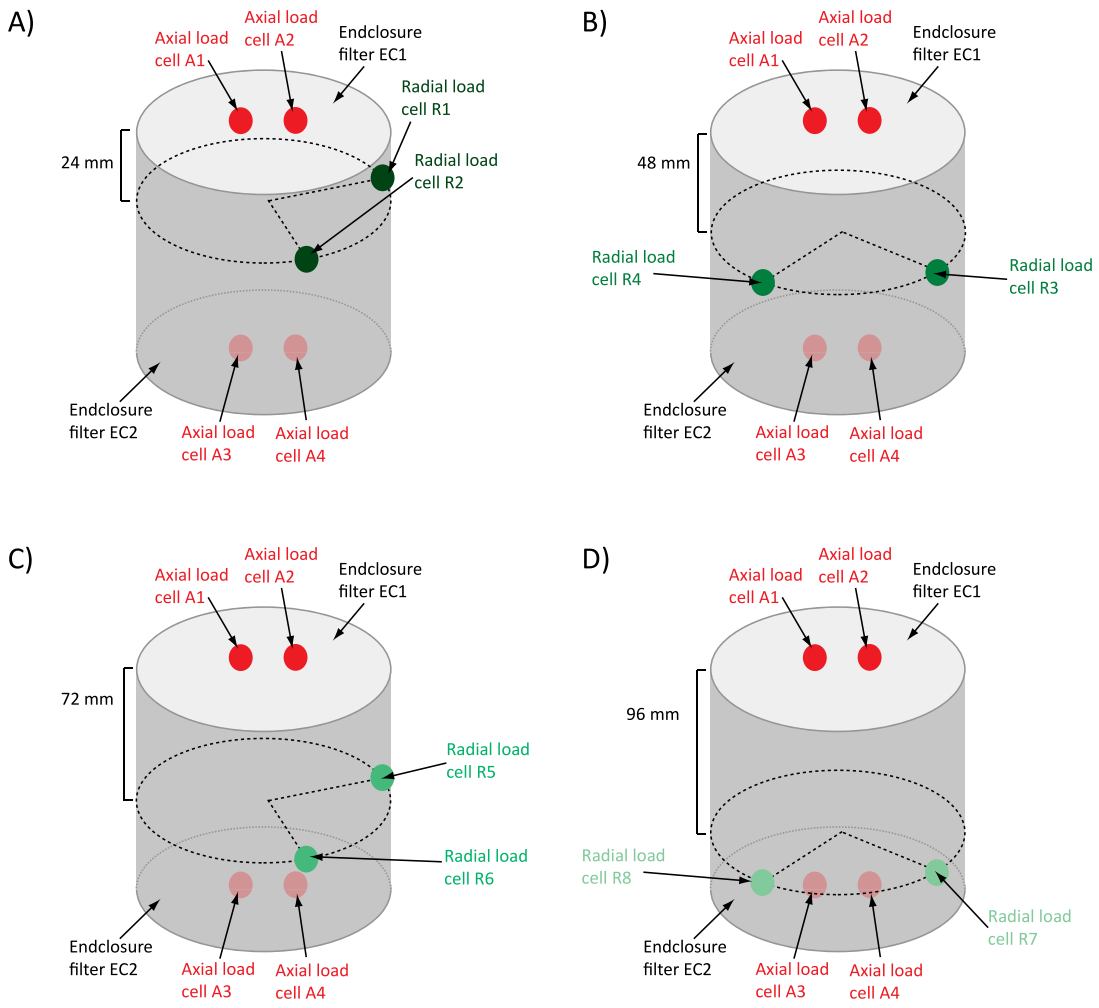

Fig. 2. Schematic diagram of sensor locations in Apparatus 1, showing the position of sensors marked along the axis of the vessel bore. Sensors located on the back of or underneath the vessel are shaded in a lighter colour.

of water during this early phase of hydration, it highlights the capacity of the bentonite to sustain significant differential stress governed by the internal shear strength of the clay. The momentary drop in pressure of R5 around day 0.2 may relate to frictional issues between the vessel wall and the clay (akin to stick–slip). However, the timing and magnitude of the drop is not directly observed in the other sensors, and may instead be explained by localised yielding of the clay. The subsequent increase in the response of the R5 sensor (increasing the difference in pressure between it and the other sensors) peaking around day 1.4, suggests simple friction and movement of the sample are not the only causes of the inflections observed in the data. Indeed, the smooth evolution of the pressure traces is contrary to classic stick–slip friction behaviour, which is signified by abrupt changes in response.[58–61] As hydration continued, swelling was focussed in radial arrays R7 and R8, which, after an initial period of anisotropy, began to converge following a similar pressure response from around day 4.5 (Fig. 4C). Sensors R7 and R8 continued to give the highest values of pressure for the remainder of the test. Close inspection of the data (Fig. 4) shows no obvious sign of stick–slip behaviour during this phase of hydration. By day 100, the rate of change in the stress had declined to a point where continued monitoring of the tests was both unwarranted and unlikely to give significant data in a practical timeframe. Furthermore, the test demonstrated that, within the prescribed timeframe of the test, closure of the initial void by swelling was possible.

Subsequent experiments with longer length samples (Test 2, Fig. 5A; and Test 3, Fig. 5B) show similar patterns for the temporal development of stress and clear anisotropy in the development of swelling pressure. In both tests, samples rapidly swell exhibiting peak swelling pressures of 3844 kPa and 4213 kPa at days 0.9 and 2.6 respectively (Table 2). These values are significantly higher than those observed in Test 1 (3307 kPa at day 1.4) reflecting the differing lengths and volumes of the clay present at the start of each test (see Discussion). Inspection of the data in Figs. 4, 5A and 5B, also reveals large instantaneous differences in stress, both across individual measurement planes and along the length of the samples. Differences in orthogonal stresses (i.e. the difference in stress between sensors on the same measurement plane) are unsurprisingly, greatest at the start when minor variations in sample geometry may impact the initial movement of water and the contact efficiency between the clay and measurement sensor. However, such issues are highly unlikely to prevail beyond the first few hours or days of testing because of the rapid swelling response of the bentonite. Even where such occurrences do exist, the bentonite must still be able to support the difference in measured stress. Fig. 6 shows the evolution in orthogonal stress during hydration and swelling in Test 1 (note: the negative values simply denote the direction of calculation as highlighted in the legend). The data clearly show that while the clay is able to support significant differential stress during the early phase of hydration, such differences quickly homogenise and by day 10, there is very little difference in stress observed across each measurement plane. In Tests 2 and 3 a similar response is noted, though the magnitude and duration of the orthogonal stresses varies slightly compared to Test 1.

While peak stress values may be influenced by initial sample geometry, because of the orthogonal arrangement of sensors, it is informative

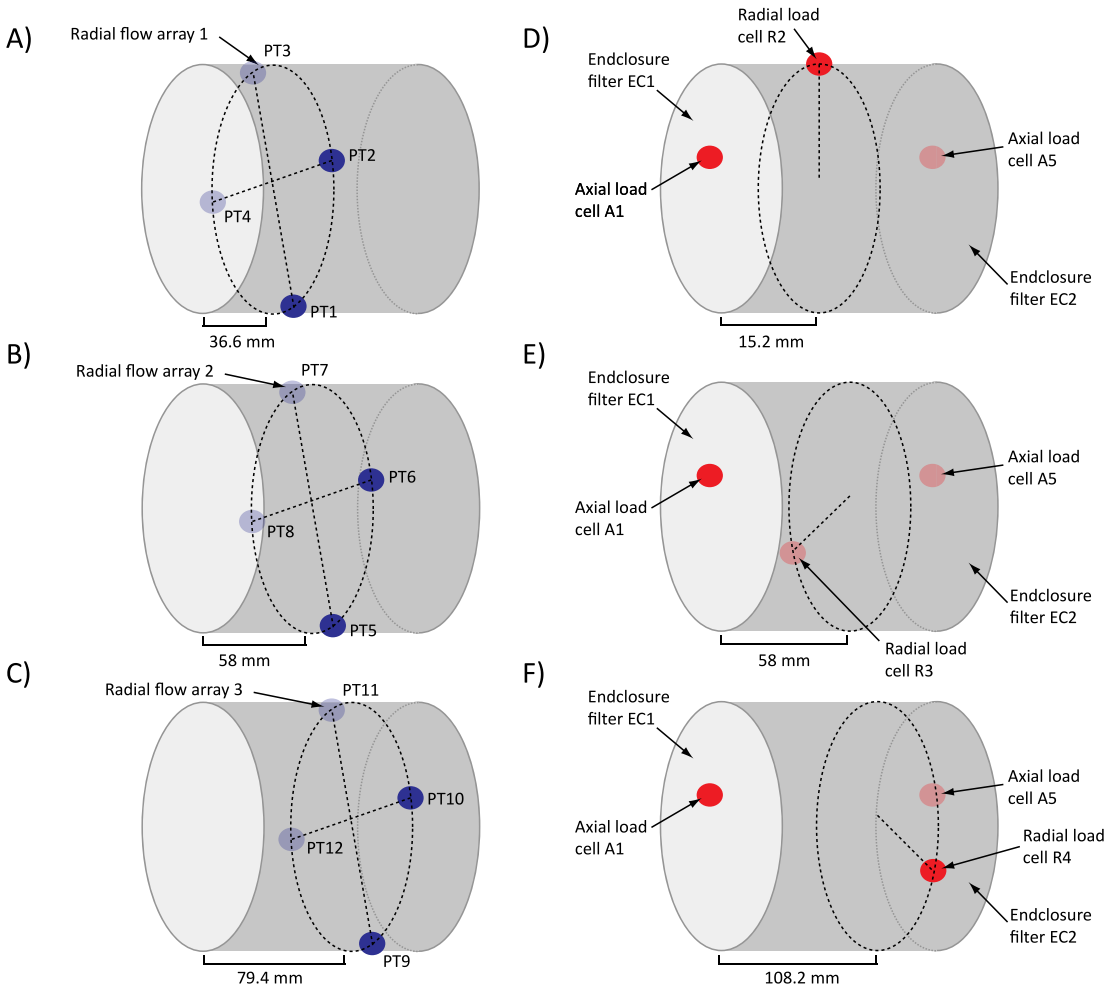

Fig. 3. The sensor locations in Apparatus 2. (A–C) Each radial flow array comprises four filters (blue dots) set at 90° to each other (giving a total of 12 points of measurement). (D–F) Five total stress sensors (red dots) are located around the periphery of the sample, two axial and three radial. Sensors located on the back of or underneath the vessel are shaded in a lighter colour.

to calculate the average value of stress at each measurement plane as a time series plot (Fig. 6). Examination of the data from each test shows a consistent response, with the development of swelling pressure initially focussed in the section of vessel containing the sample. Of more interest however, is the fact that as the sample swells, the average of values from sensors A3 & A4, R5 & R6 and R7 & R8 begin to converge and exhibit similar traces which are comparable for much of each test history. Similarly, outputs from A1 & A2 and R1 & R2 exhibit a very similar response suggesting that expansion of the bentonite is highly non-linear along the length of the vessel (see Section 3.4). Close examination of the data shows that in all three tests, stress development preferentially occurs beneath the sample (monitored by sensor A3 & A4) creating an inward force acting on the clay. This stress vector is only possible if the sample simultaneously swells in a radial direction. As the radial stress measured at the R7/R8 plane is significantly below the axial stress, radial swelling must be localised within the first 24 mm of the clay. Interestingly, in the shortest sample (Test 1), the difference between the axial stress at A3/A4 upwards to the radial stress at R5/R6 is minimal. However, from the data available it is not possible to say this behaviour is specific to this sample or representative of a trend of greater homogenisation as the ratio between sample length and void increases.

3.1.2. Tests 4 and 5 (horizontal tests)

To examine the possible effect of gravity segregation on the swelling behaviour of bentonite, two tests were undertaken in which the samples were horizontally mounted within the apparatus. Except for this geometric change, all other aspects of Tests 4 and 5 were the same as Tests 1, 2 and 3. In Test 5, the role of clay composition was examined by changing from a sodium bentonite to a calcium-rich bentonite from Bulgaria. As before, the void next to the sample was completely filled with distilled water (in both tests) by carefully tilting the apparatus during the assembly procedure. Once the final end-closure was in place, the large axial filters (EC1 and EC2, Fig. 3) were independently pressurised to 4500 kPa.

Fig. 7A shows the development of swelling pressure within Test 4 as hydration of the clay occurs. As observed before, the axial swelling pressure next to the clay (denoted Axial 1 in this test geometry) rapidly increased as the hydration started. Similarly to Test 1, the radial load cell Radial 2, located 15.2 mm from the base of the sample (next to filter EC1), quickly increased and at day 4.2 emerged as the highest response within the system. As before, this was accompanied by an increase in the Radial 3 radial sensor in the early phase of the experiment. However, unlike Test 1, before the end of day 1 the value of radial swelling pressure recorded by the Radial 3 sensor had peaked and already begun to decay. While the data is somewhat noisy, a trend of decreasing swelling pressure was then measured on the Axial 1, Radial 2 and Radial 3 sensors, which continued until around day 30. At this point, the swelling pressure reversed and began to increase once again before dropping to a low at ~day 53. This was then accompanied by the development of radial swelling pressure at Radial 4 and Axial 5 (located within and above the void respectively) to match the response seen on sensors Axial 1, Radial 2 and Radial 3 for the same time period.

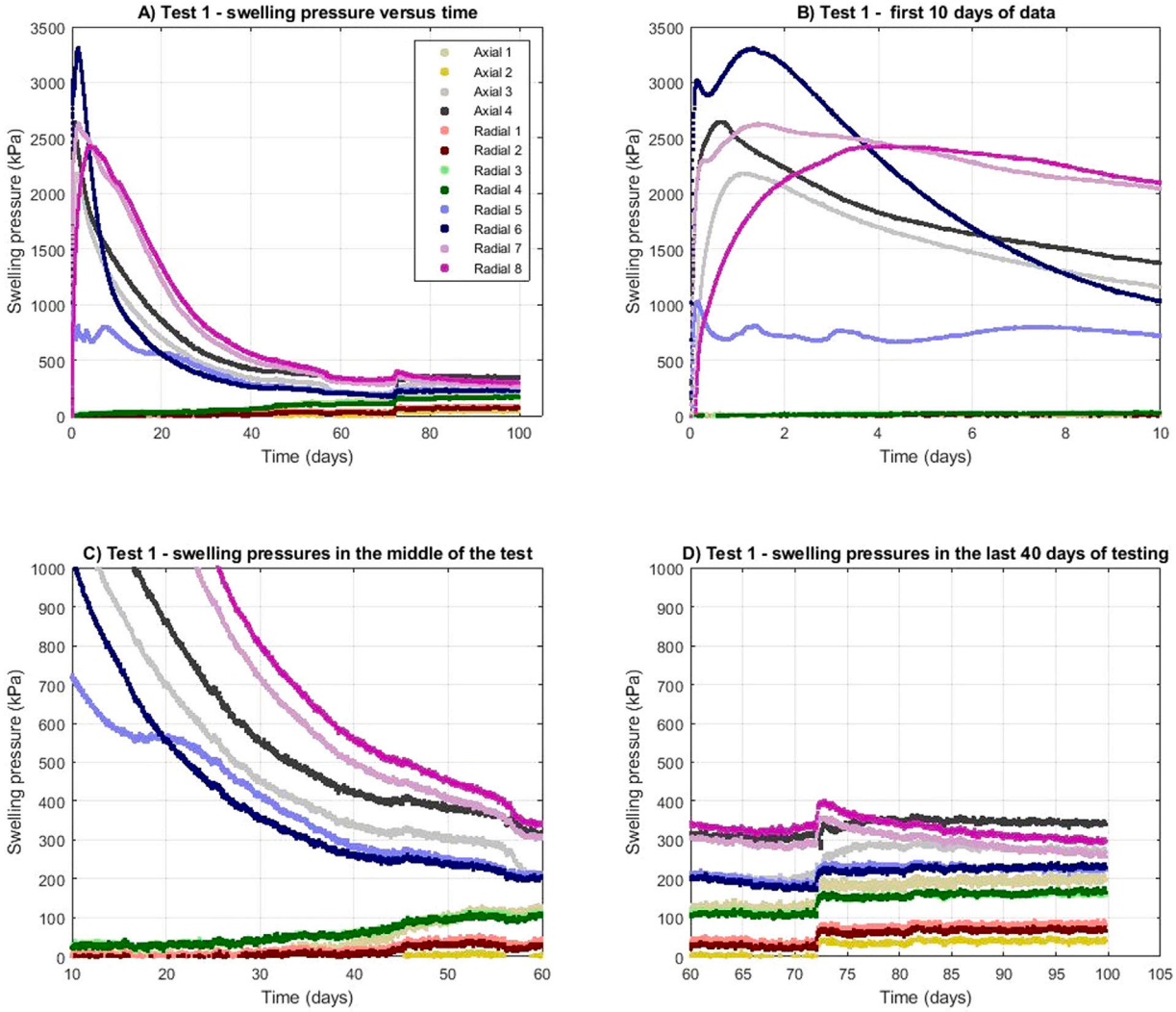

Fig. 4. (A) Development of swelling pressure during Test 1. The small drop in value from day 56.6 to 72.1 was caused when the ISCO pump controlling porewater pressure in the base of the sample was inadvertently turned off. (B) Exaggerated vertical scale showing the slow rates of pressure development before Test 1 was terminated at day 100. (C) Development of pressure in Test 1 during the first 10 days of testing. Inflections in the pressure traces may relate to friction or plastic yielding of the sample. (D) Evolution of orthogonal stress within the pressure vessel during hydration and swelling of the clay in Test 1. Note the values plotted are calculated by subtracting the readings from one sensor on a given plane from the readings of the other. To obtain only positive values for graphical purposes, the sensor on a given plane recording the smaller of the two stress values was subtracted from the sensor reading the larger of the two values. Whilst the magnitude of the value is important, the direction of calculation (as shown in the legend for each pair of sensors) is not.

Table 2
Summary of peak swelling pressures occurring during the tests, and average swelling pressures and cumulative flow data based on end-of-test values. The values in parentheses denote the sensor where the measurement occurred. The final sample dimensions at the end of each test were the same as the internal vessel dimensions as each sample had expanded to completely fill the apparatus void. The 'percentage swelling at void' is calculated by dividing the cumulative inflow volume by the starting void volume to estimate the contribution of swelling made by the clay adjacent to the void.

Test no.	Sample length (m)	Peak axial pressure (kPa)	Peak radial pressure (kPa)	Average axial pressure at test end (kPa)	Average radial pressure at test end (kPa)	Cumulative inflow (ml)	Cumulative outflow (ml)	Percentage swelling at void %
1	65.0	2647 (A4)	3307 (R6)	237	187	36.5	34.9	76.6
2	74.7	3844 (A4)	2737 (R6)	328	327	31.0	28.7	75.7
3	85.2	3948 (A3)	4213 (R6)	544	674	28.1	26.0	71.6
4	65.2	2078	1889	283	636	28.5	23.7	80.2
5	65.0	5720	4297	359	590	34.7	29.0	75.9

By the end of the test at day 76, a significant differential stress of nearly 1000 kPa remained within the vessel. This was substantially higher than that observed in either Test 1 or 2, but this may in part, reflect the precision of the measurement system in this apparatus.

Fig. 7B shows the development of swelling pressure within Test 5. In the first 20 days of testing, the swelling response of the Ca-rich clay is significantly larger than the MX80 equivalent (Test 4). However, by day 20, the swelling pressure recorded by radial load cell Radial 2, which recorded the largest swelling response, had dropped to the same magnitude as the swelling pressure seen in Test 4 (approximately 1500 kPa). As with the previous tests, at the termination point in Test 5, significant variance in the recorded swelling pressures still existed, though this may partially be reflecting the accuracy of the test. However, the rates of change in stress during the previous 40 days of

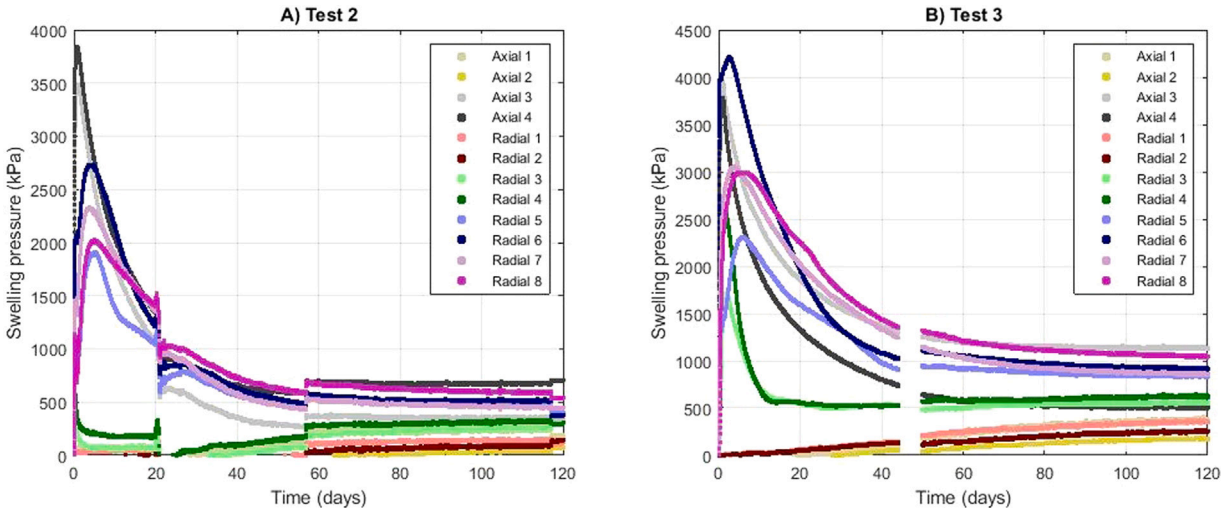

Fig. 5. (A) Development of pressure during Test 2 (sample length 75 mm). The deviation in the data collected between days 20 and 55 was due to a failure in the air conditioning system that moderates the temperature of the environmentally-controlled testing room. (B) Development of pressure during Test 3 (sample length 85 mm). A break in the data at day 44.2 to day 50.0 is caused by a breakdown in the data acquisition system.

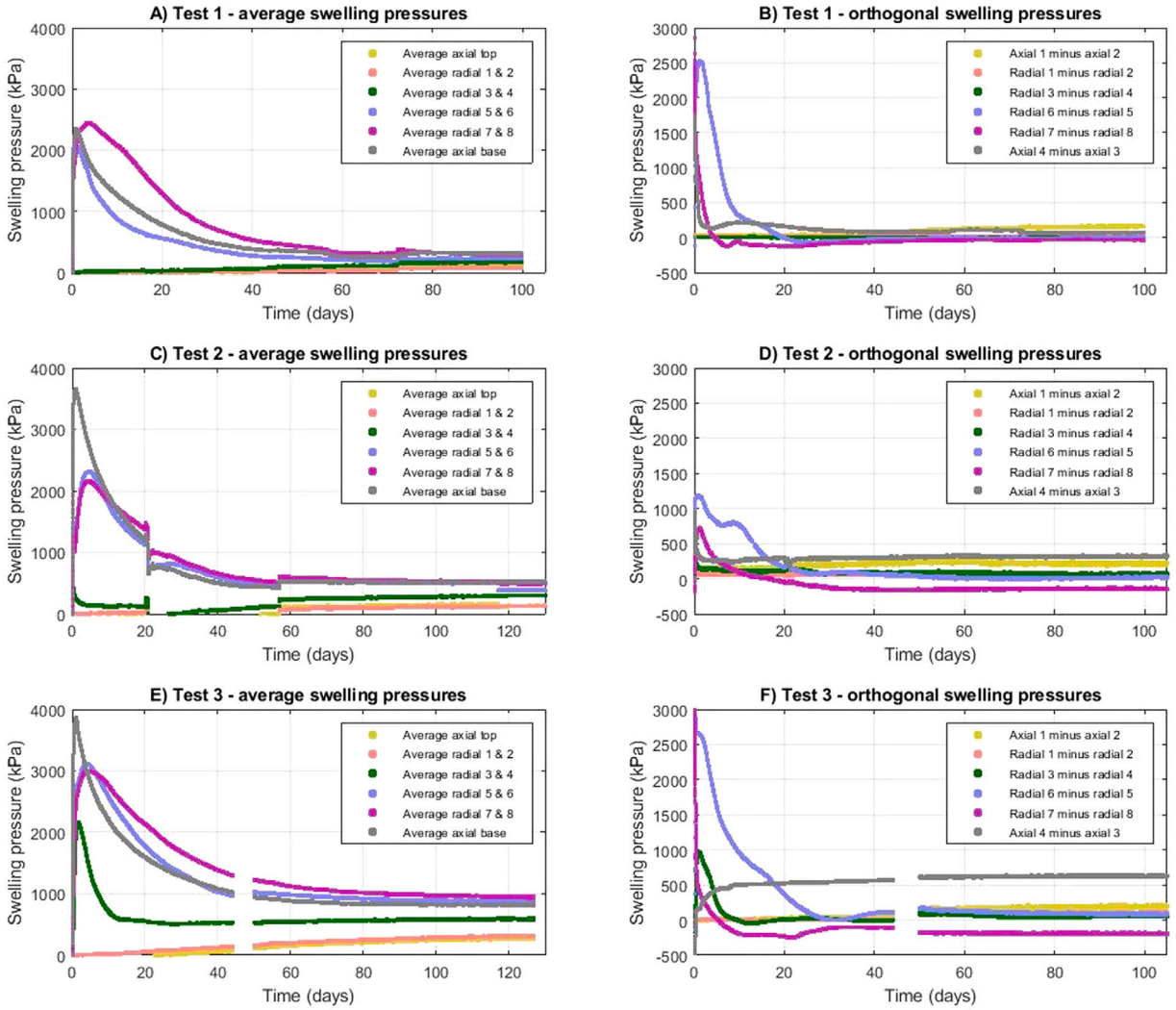

Fig. 6. (A–C) Development of average swelling pressure along the length of samples during Tests 1, 2 and 3 respectively. It is noteworthy that in all tests the average of values from A3 & A4, R5 & R6 and R7 & R8 are comparable for much of each test history, as are those from A1 & A2 and R1 & R2. The tests are plotted on the same scale for ease of comparison.

testing (day 60 to 100) were very small, suggesting the material was close to its final equilibrium state.

3.2. Water uptake

3.2.1. Tests 1, 2 and 3 (vertical tests)

In each test the cumulative flow through the base of the sample (inflow) and from the top of the vessel (outflow) were closely monitored as a function of time using a pair of highly accurate digital syringe pumps (see Section 2). In all tests a well-defined flow transient was observed (Fig. 8A), where inflow and outflow were roughly symmetrical, suggesting minimal net volume change of fluid within the vessel (<6 ml). This is not too surprising, given the void above the sample was completely filled with water immediately after installation of each sample before the end-closure was fitted. Based on comparison of the transient behaviour and asymptotic values, flux into and out of the vessel also appears proportional to the start volume of clay, with cumulative flux declining with increasing sample length. This indicates a progressive reduction in swelling strain, which is supported by the higher measurements of swelling pressure noted in Fig. 6. Data from Test 2 also demonstrate that the rate of change in the cumulative flow response is decreasing rapidly by day 100 and is minimal by the end of the test. The data in Fig. 8 also provide a useful measure with which to crudely apportion swelling strains within the sample. Examination of the data suggests around 36 ml of water entered the sample through the base of the vessel in Test 1.[2] This quantity is relatively small, compared to the start void volume of 144.2 ml, suggesting that swelling, driven by water inflow through the base of the clay, accounted for approximately 23.4% of the volume change required to close the void. As such, the bulk of the sample expansion clearly occurred through unconstrained swelling through the upper face of the clay. This accounted for around 76.6% of the swelling strains required to close the void. Post-test measurements of moisture content and dry density confirm these observations (see Section 3.4). A similar result occurred in Tests 2 and 3. Here, the proportion of swelling that occurred through water inflow from the base filter (below the sample) was 24.3% and 28.4% respectively. These values indicate that as the void length above the sample decreases, swelling above the sample is contributing less to the closure of the void.

3.2.2. Tests 4 and 5 (horizontal tests)

The cumulative flow response for Tests 4 and 5 exhibited the same general behaviour as that seen in Test 1, Fig. 8B. Examination of the Test 4 data suggests around 26 ml of water entered/left the sample through the vessel filters by the end of testing at day 76. This test was curtailed as the rate of stress change was minimal and provided an opportunity to look at potential gravity segregation effects. By the end of testing, inflow to the sample was 28.5 ml (Table 2), which compared to the same point in time, was marginally smaller than in Test 1. Using the value from Test 4, swelling through water inflow at the base of the clay, accounted for around 19.8% of the volume change required to close the void. While this value cannot be directly compared to those from Test 1 through 3, it clearly shows that, as before, the bulk of sample expansion occurred through unconstrained swelling from the upper face of the clay. This accounted for around 80.2% of the swelling strains required to close the void. Post-test measurements of moisture content and dry density again confirm these observations. The data in Fig. 8B for Test 5 shows the same response for the uptake of water as the other tests (Table 2). However, unlike in the Na bentonite experiments with similar dimensions (Tests 1 and 4), the rate of water uptake was substantially quicker in the Ca bentonite test. This lead to a well-defined asymptotic transient marking the end of hydration, and in theory, the complete homogenisation of the clay.

[2] This volume is approximate because of problems with the syringe pumps monitoring the movement of water, and as such, should be treated with caution.

3.3. Development of porewater pressure

Apparatus 2 allowed the monitoring of porewater pressure development as a function of time both within the void space of the apparatus and in the sample. Fig. 9A and B show the development of porewater pressure in Arrays 1 and 2 during Test 4. Here, water pressure can be seen to have evolved in a uniform way with the exception of filter PT6 which is atypical of the general response. In Array 1, which was closest to the end of the vessel against which the sample was placed (Fig. 3), the clay quickly swelled reducing the availability of water, leading to an initial drop in pressure. Water pressure within the filters then remained low until around day 20 when pressures gradually began to rise. While some minor anisotropy can be seen in the arrival times of the 'flood front' to each filter, the subsequent development of water pressure is similar in form and magnitude between each filter. As permeating water reached the various filters, around day 26 to 30, the pressure rapidly increased. This continued until the pressures reached around 3200 to 3500 kPa, at which point the rate of pressure increase rapidly slowed and the pressure traces adopted a much shallower gradient. The reason for the inflection in the pressure response is unknown, however, the fact it occurs in all measurement filters strongly indicates a material response to the ingress of water. Fig. 9B also shows a similar response and the same inflection in the pressure traces, albeit at a slightly higher value.

The development of porewater pressure in Test 5, performed on Ca-bentonite clay, exhibits a higher degree of anisotropy compared to that of Test 4. Fig. 9C shows that the development of water pressure in Array 1 occurs at an early time (around 15 day) compared to that of Test 4 (day 20). The development of pressure is non-uniformly distributed between the four filter measurements that form part of Array 1. Even in these small-scale experiments, the permeation of water through the clay is non-uniform resulting in considerable heterogeneity in the development of porewater pressure. Upscaling these observations suggests that localisation of flow is likely in field experiments and, as a consequence, the development of swelling pressure may be equally impacted.

3.4. Post-test analysis of the samples

Following the completion of each test, each specimen was sub-sampled to provide spatial data on the geotechnical properties of the clay. This information provided insight into the swelling response of the clay and the degree of homogenisation that had occurred during each test. Given the low strength and density of the samples, it was not feasible to directly obtain volumetrically accurate sub-samples. Instead, each sample was carefully extruded in increments using a hydraulic ram and regular slices of core were taken with a sharp blade. The slices were immediately weighed, whilst the exposed end of the sample was covered with clingfilm to minimise moisture loss. Each segment was then dried at 105 °C, and the pre- and post-test weights were used to determine the moisture content (a parameter which is not dependent on sample volume). In this way, the error in the calculation of the moisture content was minimal. A cross-plot of the moisture content data versus distance from the end of the vessel against which the samples were placed, is presented in Fig. 10. Unsurprisingly, all samples show a pronounced increase in moisture content compared to their start value, and there is a clear upward trend in moisture content increase as sample length reduces. In addition, samples with a longer starting length (Tests 2 and 3) also show slightly lower moisture contents throughout the sample length. Significant swelling is evident within the first 45–55 mm of each post-test sample, demonstrated by the three-fold increase in moisture contents in this region (Fig. 10). Here, the values are unexpectedly uniform throughout these sections of each sample. Why this would be the case is unclear. It is also interesting to note that in Test 1 there is a small but measurable increase in moisture content nearest the base of the vessel (Fig. 10A). Whilst it is not possible to say

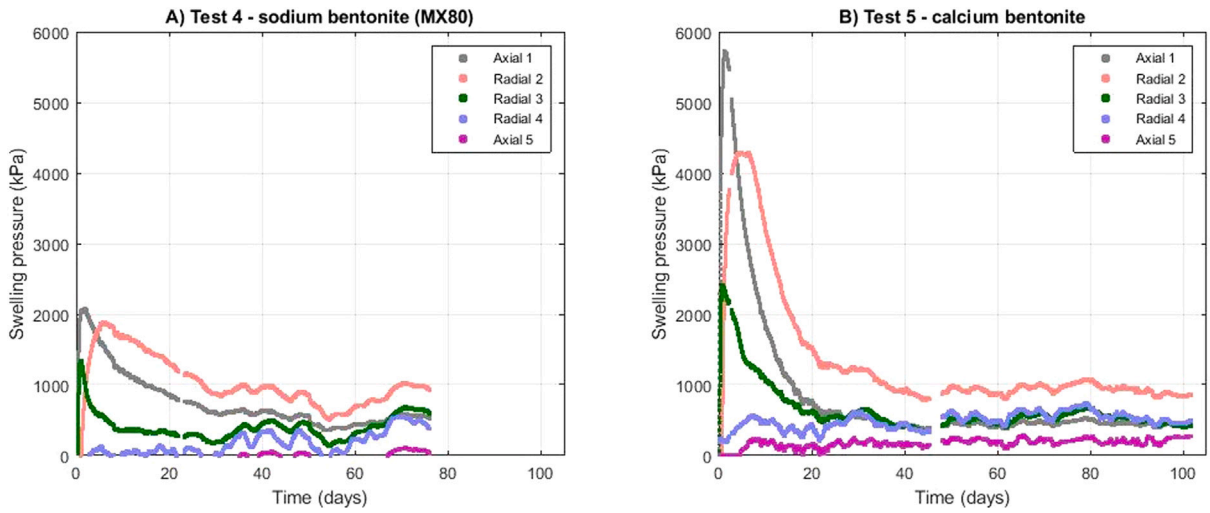

Fig. 7. (A) Evolution of swelling pressure during Test 4 where the sample was mounted in a horizontal position. (B) Evolution of swelling pressure for the Ca bentonite Test 5. The tests are plotted on the same scale for ease of comparison.

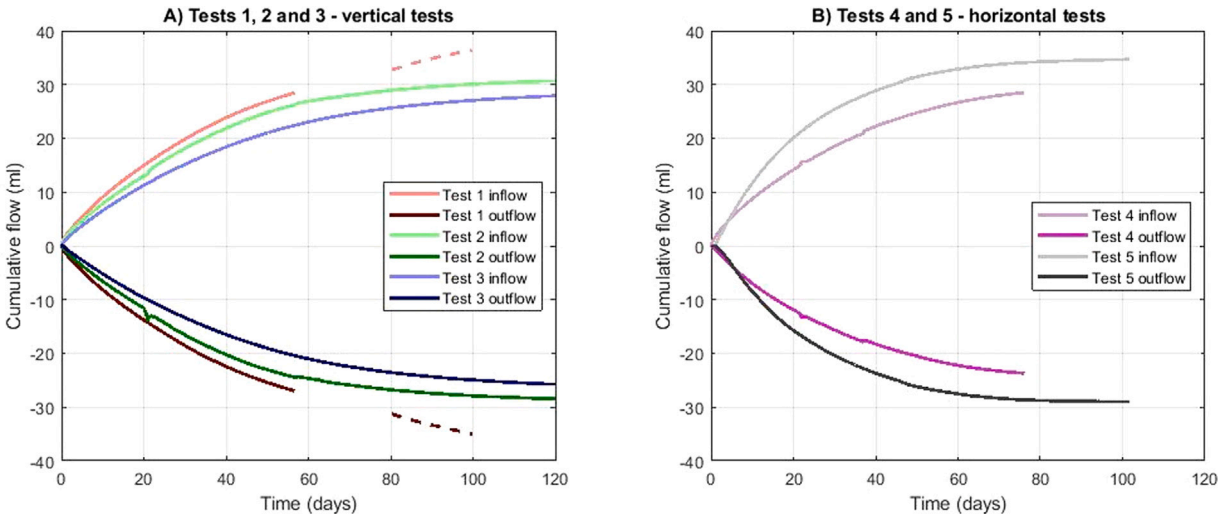

Fig. 8. (A) Cumulative flow into and out of the vessel from below and above the core, for Tests 1 to 3. The flux in Test 1 from day 80 to the end of the test is marked by a dashed line because it is approximate and should be taken with caution. (B) Cumulative flow from Tests 4 and 5 added to the data from (A).

for certain, it seems likely this increase was caused by an initial uplift of the sample as axial stress developed more rapidly than radial stress during the very early stages of the experiment (Fig. 4).

Inspection of the data shows that large gradients in moisture content were only observed in the volume originally occupied by the void. This latter observation is to be expected as progressive unconfined swelling of the clay occurred into the void. This is also supported by the cumulative flow data presented in Section 3.2 which suggests that around 70%–80% of swelling occurred through water uptake from the top face of the clay. Fig. 10B shows moisture content data from the two horizontal experiments (Tests 4 and 5). From 0 to 100 mm, the data from Test 4 is very similar in form and magnitude to that of Test 1 (Fig. 10A). However, from 100 to 116 mm the moisture content values for Test 4 increase rapidly compared to those of Test 1, though the reason for this behaviour, given the same composition and similar dimension of the samples, is unclear. To examine the possible effects of gravity on the swelling behaviour of the bentonite, the core from the horizontal tests, was also slabbed at its mid-plane to provide two estimates of moisture content, one in the upper half of the clay and the other in the lower half (Fig. 10B). Whilst the moisture content values are consistent in each half of the Test 4 sample through much of its length, as moisture contents increase above approximately 150% the data diverges providing clear evidence of gravity segregation present in these high moisture content sections of the clay. The longevity of these differences cannot be derived from the current data and further work is required to define the evolution of this long-term behaviour.

The Ca-bentonite sample (Test 5) exhibited similar moisture content values to Test 4 for the first half of the sample length (0–58 mm), and after this point in the sample, showed increasingly lower values (Fig. 10B). Such observations suggest that significantly less swelling and thus homogenisation of the clay, occurred in the upper half of the Ca-bentonite sample. However, above 100 mm the Ca-bentonite sample showed very large moisture content values, most especially at the top of the void and in the top half of the sample. This provides strong evidence for gravity segregation in this sample during swelling.

4. Discussion

It is clear from the data presented in Figs. 4, 5, 6 and 7, and from the post test measurements of moisture content (Fig. 10) that in all tests the bentonite is able to swell and completely fill the initial starting void, creating a small but measurable axial stress within 100 days (or less) of testing. It is also clear that during the swelling process,

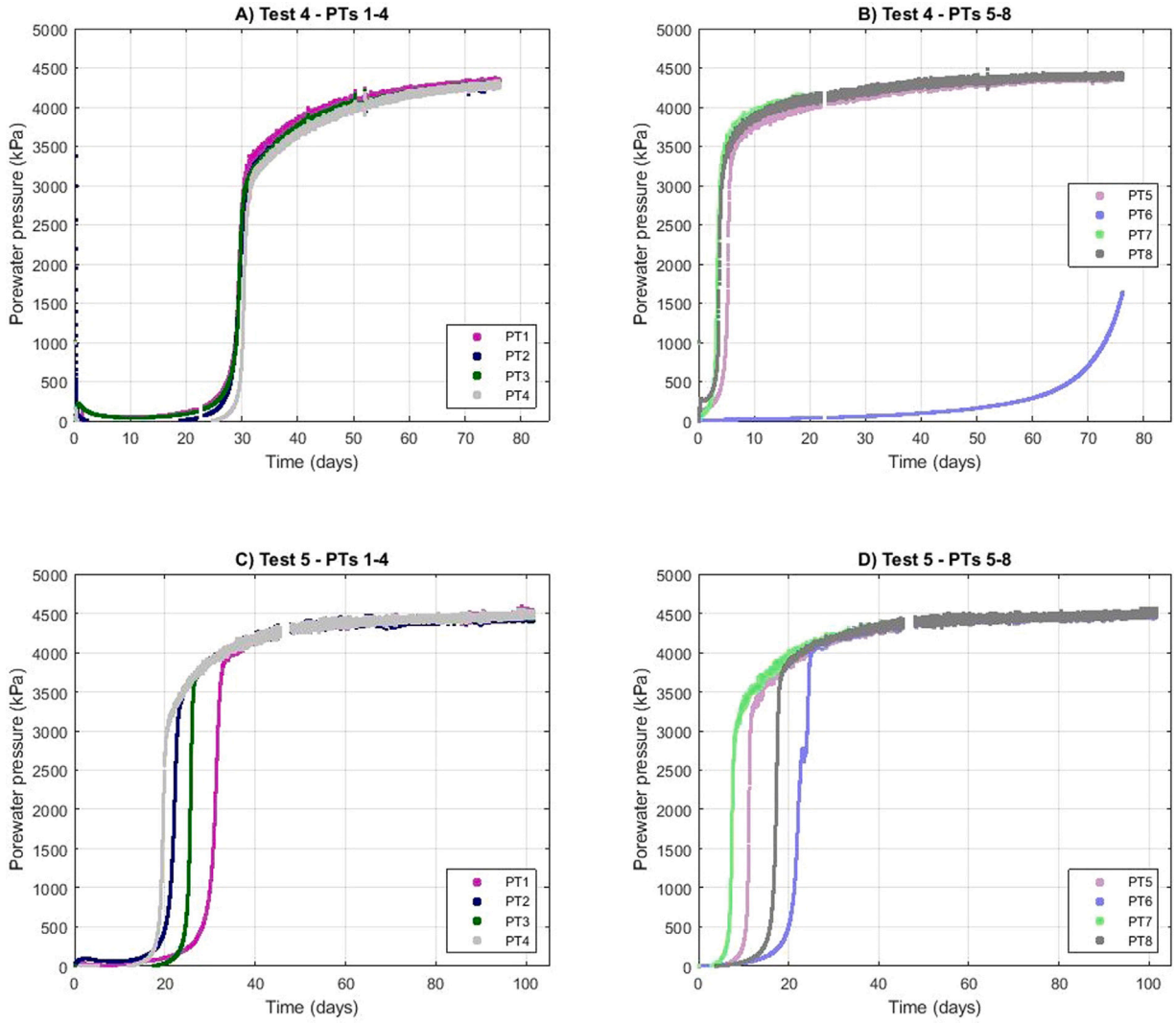

Fig. 9. Development of porewater pressure in Arrays (A) 1 (closest to the end of the vessel against which the samples were placed; PT1, PT2, PT3, PT4) and (B) 2 (at the midplane of the vessel; PT5, PT6, PT7, PT8) during the hydration in Test 4. (C) and (D) show the same responses but for Test 5.

complex changes in the composition (i.e. ratio of clay to water) and distribution of clay within the apparatus occurs. The compilation of flow data presented in Fig. 8B indicates a systematic trend in water uptake/discharge dependent on the start length of the clay. While cumulative flow decreases as sample length increases, flows into the horizontally mounted sample (Test 4) appear systematically smaller than the equivalent vertically orientated sample (Test 1). Results from Test 4 also exhibit slightly lower moisture contents in the section of the vessel occupied by the original sample, compared to equivalent values from Test 1. Clay with a lower moisture content should exhibit a larger average swelling pressure (for a saturated sample) and indeed, higher residual stresses are observed at the end of Test 4. This slight difference in moisture content also corresponds with a lower flux into the sample and out of the vessel in Test 4 than in Test 1; the cause for this response is unknown. It seems unlikely that gravity is the culprit for the higher residual stresses in Test 4, as the additional pressure component derived from gravitational acceleration is minimal compared to the stresses developed in the apparatus. While based on only two measurements, the moisture contents derived from clay material that swelled into the void are substantially higher in the horizontal (Test 4) than in the vertical experiment (Test 1). While there is clear evidence of gravity-induced settlement of the clay, the cause for the increase in moisture content in the horizontal test is unclear; the moisture content differences are sufficiently large to exclude experimental error. The limited data presented as part of this study suggests that gravity segregation effects are much stronger in the Ca-bentonite sample (Test 5) than in the Na-bentonite sample (Test 4). It seems unlikely that this directly relates to the swelling capacity of the clay as the final swelling pressures (Table 2) were very similar. However, the decrease in moisture content in the lower half of the Ca-bentonite samples, may reflect settlement of the heavier clay fractions and detrital material contained within the clay fabric. This would likely result in a 'locked-in' heterogeneity which may impact the long-term homogenisation of the clay.

Fig. 11 shows a compilation of data from all five tests in which the swelling caused by the total uptake of water (ml) through the base of the sample, expressed as a percentage of the initial volume of the starting void, is plotted against initial void length. While some scatter exists in the data, probably caused by the different accuracy and instrumentation densities between the two apparatus systems (see Section 2), a clear negative trend in the data is observed. This indicates that as void length increases so does the contribution of swelling from the sample face adjacent to the void.[3] This is evident in the post-test moisture content profiles (Fig. 10), which show progressive increases

[3] There is insufficient data to accurately extrapolate the intercept of Fig. 11, but at zero void length, the component of swelling from each end of the sample would be expected to be 50%.

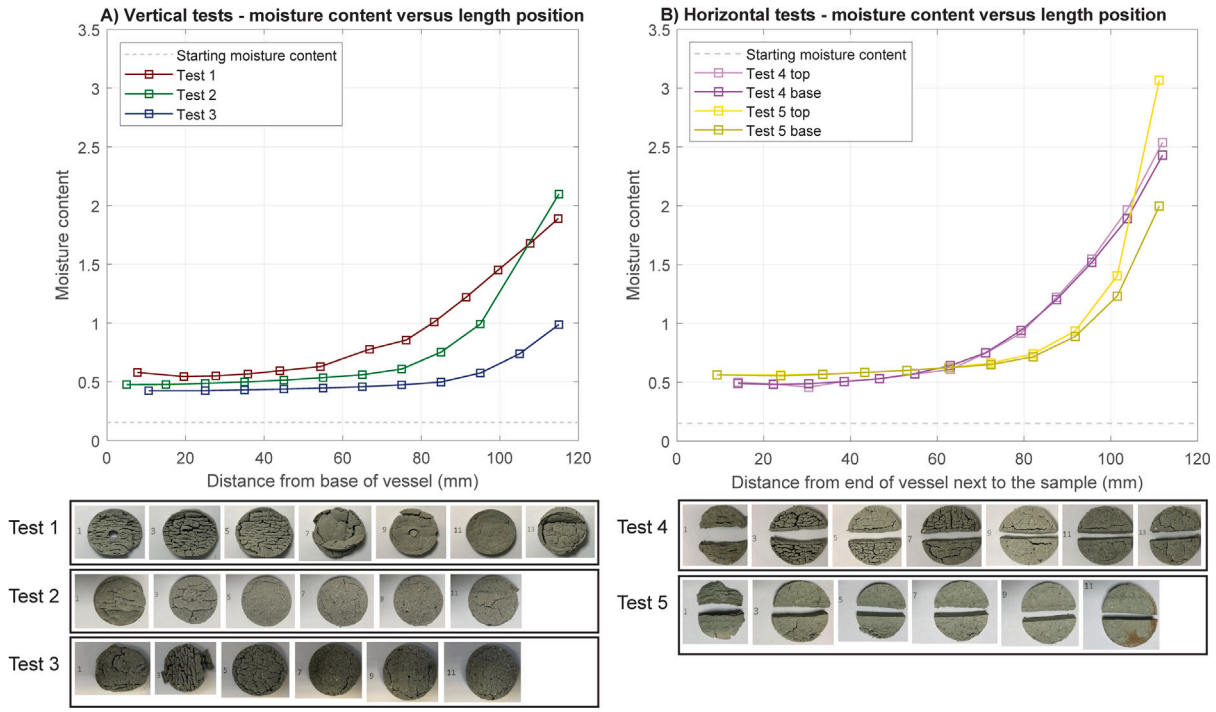

Fig. 10. Cross-plot of moisture content against distance from the base of the vessel for (A) Tests 1 to 3, and (B) Tests 4 and 5. In the horizontal tests (Tests 4 and 5), the base is equivalent to the end of the vessel against which the clay was placed prior to testing.

in moisture content at shorter distances along the length of the vessel. This nicely highlights the role of stress and friction, in this case between the clay and vessel wall, and its capacity to limit swelling from the face of the clay adjacent to filter EC1.

A compilation of the average swelling pressure data is presented in Fig. 12. While pressure data generated by Apparatus 2 (Tests 4 and 5) is noisier than for Apparatus 1 (Test 1 to 3), similar trends in behaviour are observed throughout the Na-bentonite experiments (Tests 1 to 4) (Figs. 12A–C). Examination of the data suggests stress gradients exist along each sample, with average values of stress lowest at the end of the vessel next to the void. While the shape of the pressure response for axial and radial swelling pressure varies between tests (Figs. 12A and B), all traces begin to approach a well defined asymptote by around day 100. In a long duration test (> 700 days) reported by Harrington and co-workers,[62] persistent residual stresses were observed in a sample with a starting void length of zero, which if correct suggests equilibration times of many years. At 100 days in the current testing schedule, the rate of change in stress has now reduced to such a level that it is unclear how long it would take for each experiment to homogenise, if such an end-point was even possible. Indeed, the 18 year FEBEX test programme demonstrated that homogenisation ceased quite early in the hydration process, and there was no appreciable change in the dry density gradient between 5 and 18 years.[27]

Test data also exhibit significant differential radial stresses particularly during the early stages of testing (Figs. 4, 5, 6 and 7) with measured orthogonal stresses in excess of 2000 kPa (Fig. 6). Axial expansion of the clay is clearly limited by the development of radial stress, which through friction with the vessel walls (mentioned above), prevents expansion of the clay at its base. However, the development of large orthogonal stresses suggests that the permeation of water may not be uniform within the sample. While no porewater pressure data is available for Tests 1 to 3, data presented in Fig. 9 confirms that water permeation is spatially complex and can be both relatively uniform (e.g. Test 4) or nonuniform (e.g. Test 5). The development of porewater pressure also varies temporally with inflections in the rate of pressurisation evident in the data. The cause for this behaviour is unclear but as porewater pressures begin to homogenise within the sample (Fig. 9C and D), the magnitude of the differential stresses also reduces (Fig. 7). While the availability of water emerges as a key consideration in the development of homogeneous stresses, the magnitude of any differential stresses cannot exceed the local shear strength of the clay. If this was to occur, then shear planes would develop and the measured differential stresses observed during testing would rapidly decrease. While there is no evidence for such macroscopic features in either the swelling pressure or flux data, the significance of shear strength and the rheological properties of bentonite in the persistence of the residual stresses noted at the end of each test, cannot be discounted. Regardless, the existence of residual stresses and the slow rates of homogenisation in the development of porewater pressure, suggest full homogenisation of the clay, accompanied by equilibration of porewater pressure, is a very slow process indeed, as supported by Harrington and co-authors.[62]

Interestingly, there is no obvious evidence for classic 'stick–slip' behaviour in the data caused by the frictional interaction between two surfaces, in this case the clay and vessel wall. The lack of such observations suggests that expansion of the clay is one of smooth transition, gently and continuously expanding into the void over time. That said, clay particles adjacent to the vessel walls should not be considered stationary and stuck to its surface, but quite the opposite. Fig. 13 shows a post-test image of a test sample having been removed from the apparatus. Faintly visible is the remains of a black arrow drawn on the original sample which has been elongated as the clay has swelled into the void. This simple qualitative observation demonstrates that the clay (and the ink of the arrow) can slide along the interface between the clay and steel, without the need of stick–slip behaviour. However, it seems probable that as surface roughness of the interface increases, friction may play a more dominant role in the mobility of the clay adjacent to that surface.

In Fig. 14 the movement of particles has been directly measured using a Geotek Rotating X-ray Computed Tomography (CT) scanner. Here the position of small lead shots placed in the sample during manufacture, have been tracked through pre- and post-test imaging. The pre-test image clearly shows the concave nature of the layers of lead, caused by the compression of the sample during compaction and resulting friction with the vessel wall (Table 3). This is illustrated

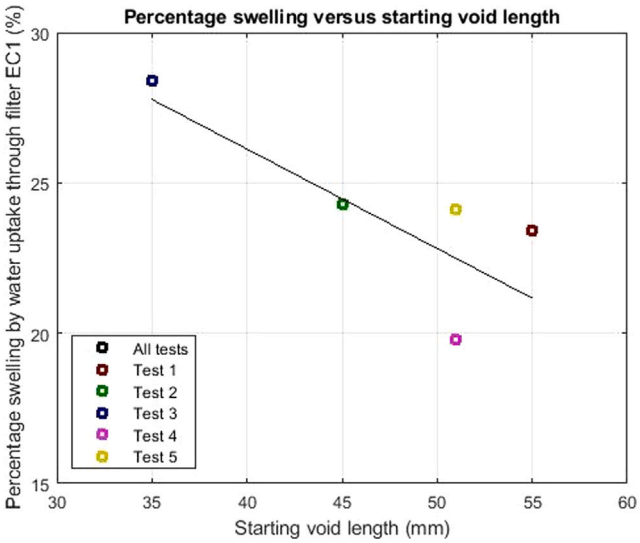

Fig. 11. Percentage swelling through water uptake from the filter (EC1) next to the clay plotted against initial void length. Test 5 is not included in the derivation of the trend line as this experiment was performed with Ca-bentonite. If only data from the vertical tests were used for fitting, the trendline would plot slightly higher at its right-hand end, and closer to the datapoint for Test 5.

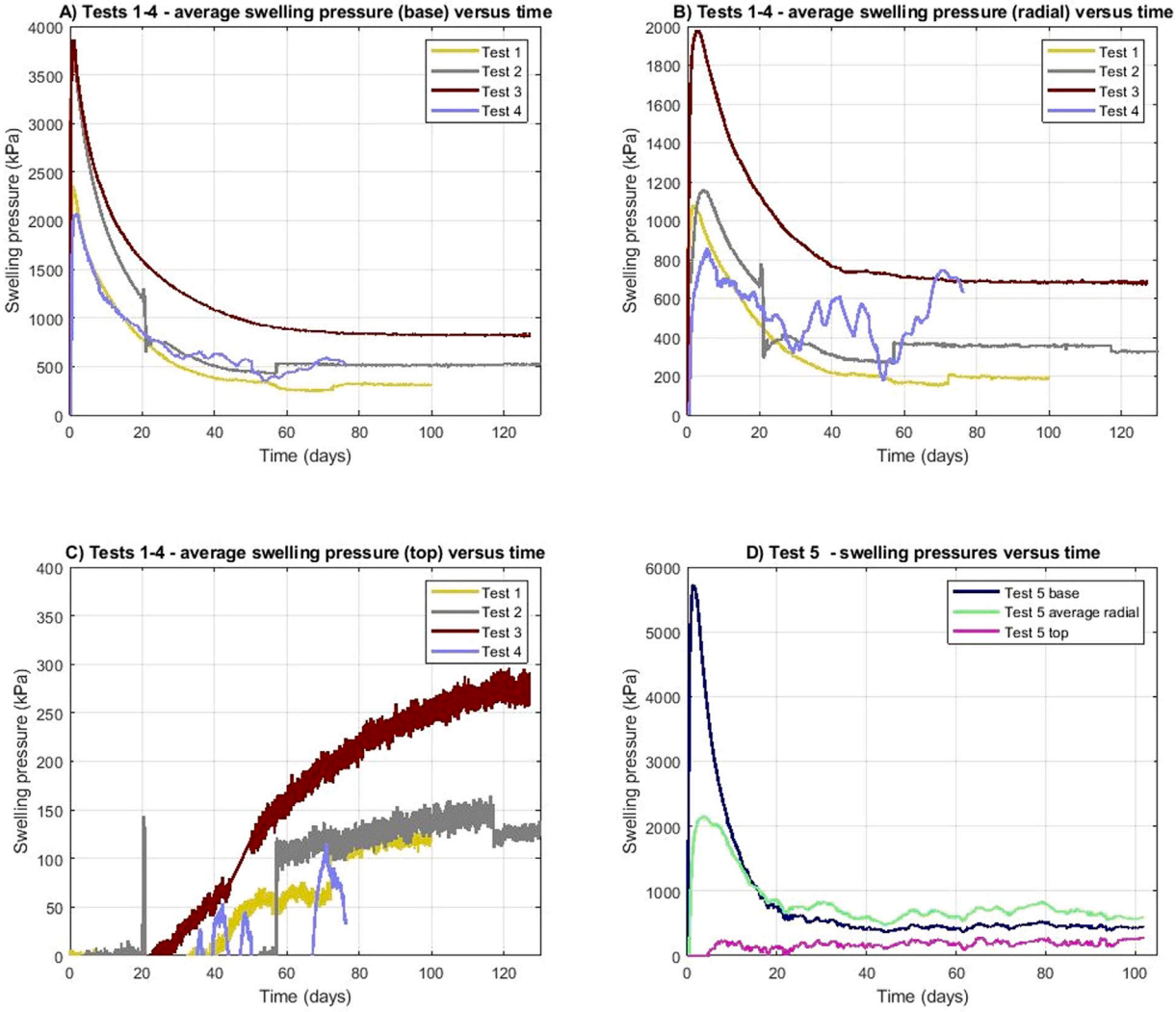

Fig. 12. Compilation of data showing the average base, radial and top swelling pressures for Na-bentonite Tests 1 to 4 in (A), (B) and (C) respectively. At day 44.2 to day 50.0 there is an interruption in the data acquisition for Test 3. (D) shows the same data but for the Ca-bentonite experiment (Test 5).

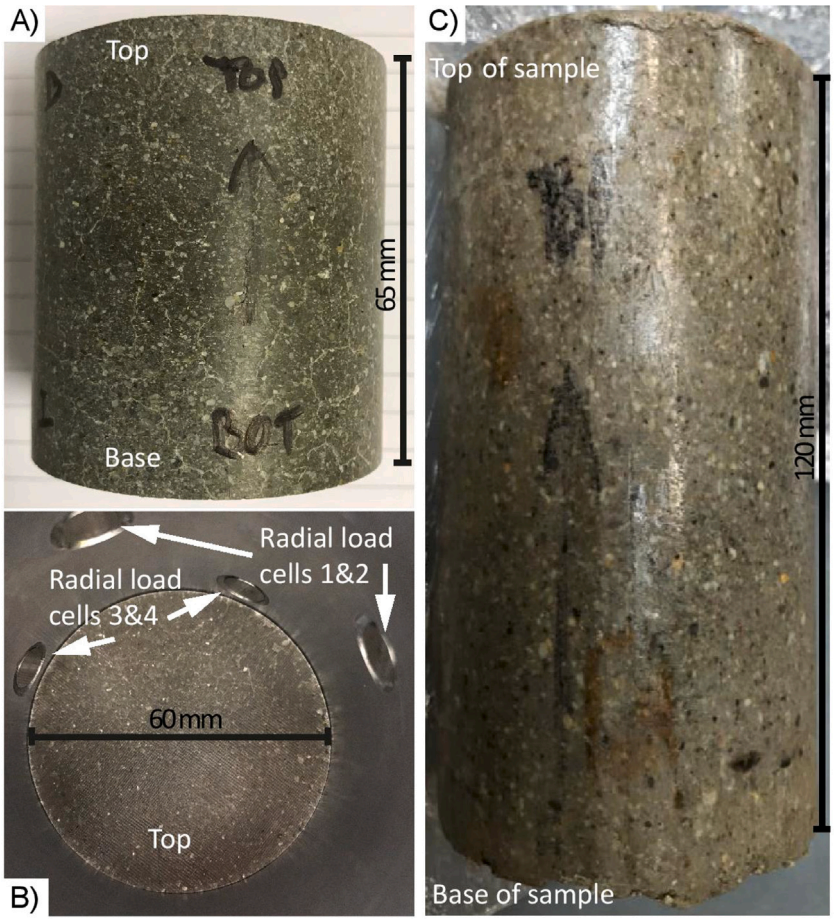

Fig. 13. Photographs of the pre- and post-test sample from Test 1. (A and B) Pre-test photographs of the sample showing the top and sides, with an arrow drawn onto the clay to show the upwards direction. (C) The sample sited in the vessel before testing began, showing the positions of the Radial load cells 1–4 in relation to the initial sample length and starting position. (D) Post-test sample after removal from the apparatus at the end of Test 1.

by an increase in concavity in the patterns of lead shot towards the base of the pre-test sample. The difference in the size of the samples before and after testing reflects the volume change during testing due to swelling. The difference in the layer numbers, along with the known layer thickness from the CT scanning, can be used to quantify the swelling between lead layers (Table 3). Each scan equates to a thickness of 8.8 μm, providing a resolution limit caused by averaging the data within a single plane. Based on the analysis of the results (Table 3), swelling of the clay occurred primarily towards the base of the sample and whilst the post-test concavity is slightly reduced throughout, the reduced concavity is also more pronounced towards the base. The small overall reductions in concavity suggest that, as slightly more of the expansion has taken place in the centre of the sample, friction on the sidewalls may have played a very minor role in slowing the sample expansion at the edges. Equally, the reduction in concavity can be explained by the uneven distribution uptake of water through the base, as indicated in Fig. 9. This is to be expected as water was only introduced (at a fixed flow rate) through filter EC1 located beneath the sample. A progressive decrease in volume (i.e. swelling strain) between the measurement layers from the base to the top of the sample is inferred. No discernible change in volume was observed between the top of the sample and the first layer of lead shot (CT layers 23 to 161 and 25 to 161 respectively; Fig. 14) which indicates the limit of water movement within the bentonite sample. Similarly, a cross plot of the pre- and post-test difference data against post-test sample length show a well defined linear swelling profile within the sample (Table 3, Fig. 14C). Visual inspection of Fig. 14C confirms this observation, and clearly shows that the patterns of lead shot retain their shape and relative positions within each reference plane. This indicates that swelling is fairly uniform and that clay particles are free to move and not impaired by side-wall friction in any significant way. The free movement of clay during swelling is an important observation, and suggests side-wall friction can be ignored during bentonite swelling.

The expected inverse relationship between moisture content and swelling pressure is crudely illustrated in Fig. 15. As moisture content increases, a general trend of decreasing swelling pressure is observed. However, the correlation between values is poor indicating the measured value of swelling pressure is not simply a function of the local moisture content. This discrepancy can be linked to the geometry of the test and the imposition of a constant volume boundary condition. As samples swell and clay fills the start void, reflective stress may be generated as clays in higher density zones continue to swell and act against the lower density clay resident in the engineering void. If such a process occurred in this type of constant volume experimental configuration, it could skew the relationship between moisture content and measured swelling pressure. Such a disparity would continue until full homogenisation of the clay and porewater had occurred. Since this is not the case in the data presented, homogenisation of the samples is incomplete.

The aim of this experimental study was to examine the swelling capacity of bentonite and ascertain if, under extreme sample-to-void ratios (1:0.85), bentonite was able to fill engineering voids, retain some form of cohesion through the development of measurable swelling pressure and ultimately homogenise throughout the test space. Fig. 16 shows a series of summary plots of final average swelling pressures as a function of void length for Tests 1 to 3. Fig. 16A shows that as void

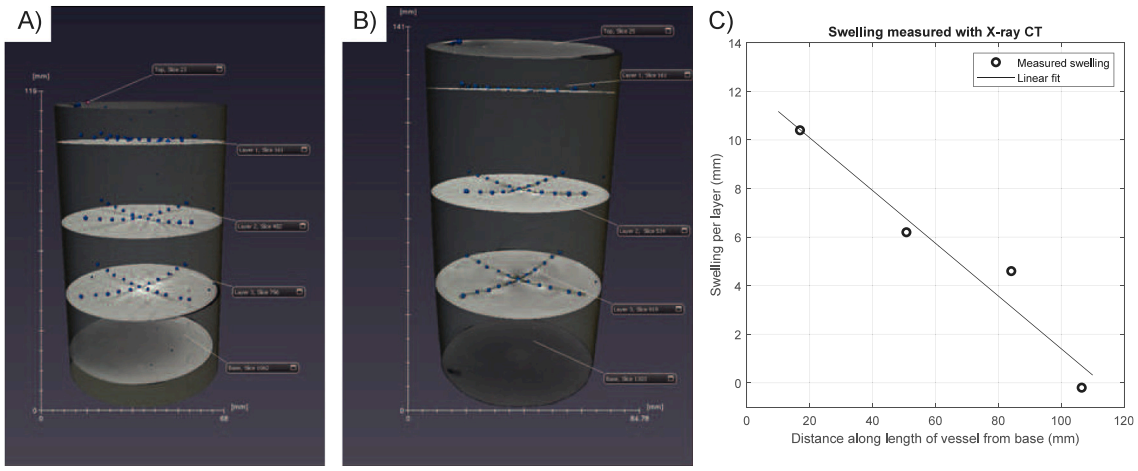

Fig. 14. (A) Pre and (B) post-test CT-images of a sample containing small lead shot. The sample was only hydrated from its base which explains why swelling occurred primarily in this region. (C) Sample length change as a function of the position along the sample, averaged for the 4 layers imaged by X-ray CT.

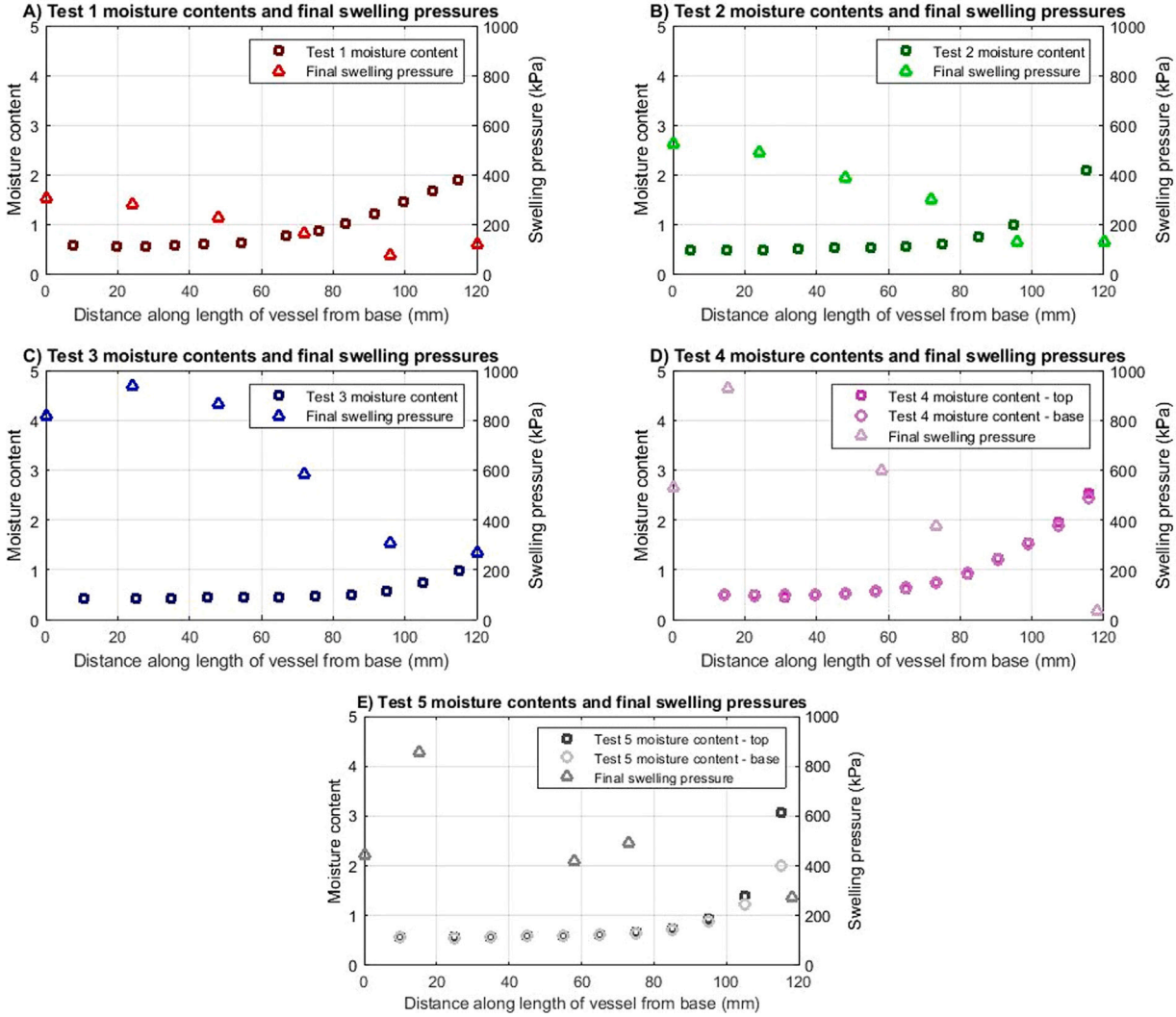

Fig. 15. Moisture content and swelling pressure plotted against (A–C) distance along the length of the vessel (from its base) for Tests 1 to 3, and (B) distance along the length of the vessel from the end against which the sample was placed at the start of testing for Tests 4 and 5.

length increases, swelling pressures become more evenly distributed along the final length of the apparatus. Conversely, as void lengths reduce, the distribution in swelling pressure is biased towards the base of the samples. This homogenisation of swelling pressures is evident in Fig. 16B, which also exhibits a clear inverse relationship between

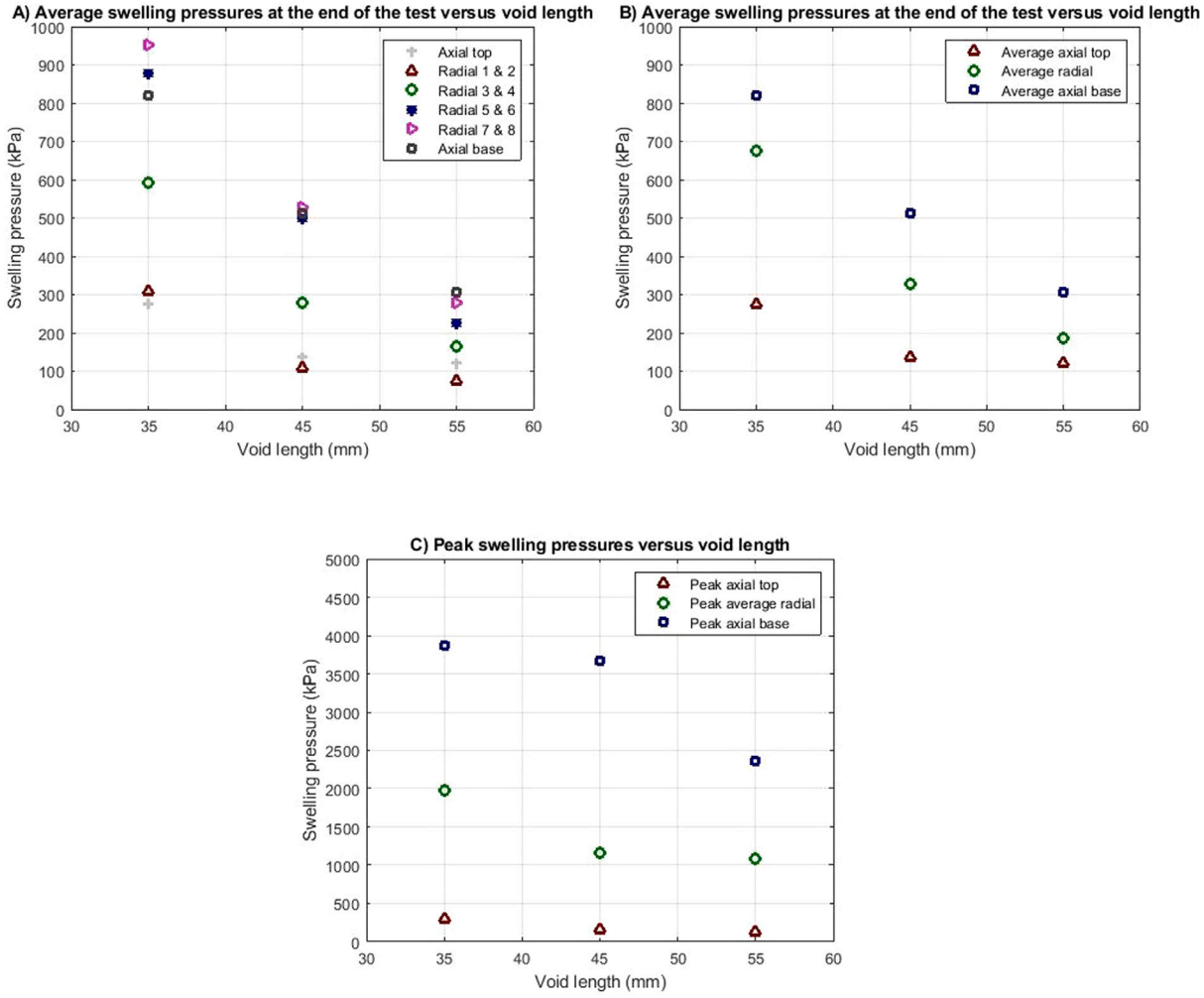

Fig. 16. Averaged swelling pressures at the end of each test plotted against void length, for Tests 1 to 3. (A) Averaged axial and averaged radial values for each plane of measurement within Apparatus 1. (B) Averaged axial top, averaged radial and averaged axial base values. (C) Averaged peak axial top, averaged peak radial and averaged peak axial base swelling pressures.

Table 3
Quantitative analysis of lead shot layers gained from pre and post-test CT analysis. The difference in layers is calculated by subtracting the current CT scan layer number for a particular lead shot layer from previous value. The concavity value represents the difference in height between the lead shot at the edge of the sample and that in the centre. The error in the concavity measurement is estimated to be ±0.02 mm.

Pre-test					Post-test					
Lead shot layer	CT scan layer	Diff. in layers	Dist. between layers (mm)	Concavity (mm)	Lead shot layer	CT scan layer	Diff. in layers	Dist. between layers (mm)	Concavity (mm)	Pre- and post-test diff. (mm)
Top	23	0	0		Top	25	0	0		0
1	161	138	12.1	0.21	1	161	136	12.0	0.16	−0.1
2	482	321	28.2	0.36	2	534	373	32.8	0.33	4.6
3	796	314	27.6	0.43	3	919	385	33.9	0.33	6.3
Base	1062	266	23.4		Base	1303	384	33.8		10.4

swelling pressure and start void length. Even at extreme sample-to-void ratios, the bentonite is able to completely fill the void, retain cohesion and create a measurable swelling pressure. This consistency in behaviour also extends to peak swelling pressures (Fig. 16C), where the highest average values are always observed at the base of the sample. More data is required to delineate the relationships beyond the three data points presented. However, the information derived from this study suggests simple functional relationships describing the swelling potential of bentonite across different engineering voids is both possible and straightforward.

5. Conclusions

Five homogenisation tests have been successfully performed on pre-compacted samples of Na- and Ca-bentonite, which have been allowed to swell into a fixed volume void. Results demonstrate that even under extreme bentonite-to-void ratios, the bentonite is able (under zero hydraulic gradient) to swell and ultimately fill each void, creating a small but measurable swelling pressure. The development of swelling pressure is spatially complex and time-consuming, exemplified by the existence of persistent differential stresses at the end of testing and

the slow equilibration of porewater pressure. Friction, manifest through classic 'stick–slip' behaviour, appears not to play a role in the development of stress and mobility of clay, where expansion of the bentonite is one of smooth transition, gently and continuously expanding into the void with the passage of time. Instead the shape and form of the stress traces suggest swelling is characterised by plastic yielding of the clay. Where water is available at both ends of the sample, the majority of swelling and water uptake occurs through unconstrained swelling adjacent to the engineering void. In these experiments this accounts for around 70%–80% of the strain required to close the void. However, the availability of water and the development of radial stress early in each test strongly influences the swelling behaviour of the clay. Pronounced increases in moisture content were measured but poorly correlated to the development of stress. Evidence of gravity segregation was also present in tests performed horizontally, with effects more pronounced in the Ca-bentonite test. The presence of gravity segregation may result in a 'locked-in' heterogeneity, which would impair both the swelling potential and homogenisation of the clay. In combination, the moisture content results, persistent differential stresses and the development of porewater pressure indicate a non-equilibrium system, the end-point characteristics of which are unclear and will take many years to homogenise at a minimum, if homogenisation occurs at all. However, these experiments clearly demonstrate that it is possible and straightforward to define simple functional relationships describing the swelling potential of bentonite across different engineering voids.

Declaration of competing interest

The authors declare that they have no known competing financial interests or personal relationships that could have appeared to influence the work reported in this paper.

Acknowledgements

This study has been funded by the European Commission through the Euratom programme and the BEACON (Bentonite Mechanical Evolution) Project (EC Project no. 745942). Funds to cover the costs of gold route open access publishing were provided by SKB. The authors thank Robert Cuss, Fiona McEvoy and Elena Tamayo-Mas of the British Geological Survey for their helpful reviews of earlier versions of this manuscript. Simon Holyoake is thanked for his assistance with instrumentation and data acquisition. Humphrey Wallis and Wayne Leman are thanked for the design and manufacture of the experimental apparatus and the careful preparation of the samples. This paper is published with the permission of the Director of the British Geological Survey.

References

1. Sellin P, Leupin O. The use of clay as an engineered barrier in radioactive waste management—A review. *Clays Clay Mineral*. 2013;61:477–498. http://dx.doi.org/10.1346/CCMN.2013.0610601.
2. Johansson E, Siren T, Kemppainen K. *Onkalo – Underground Rock Characterization Facility for in-situ Testing for Nuclear Waste Disposal*. International Society for Rock Mechanics and Rock Engineering, 13th ISRM International Congress of Rock Mechanics, 10-13 May, Tech. Rep. IDISRM-13CONGRESS-2015-200, Montreal, Canada: 2015.
3. Waste Isolation Pilot Plant UDoE. WIPP Site.
4. Chapman NA. Geological disposal of radioactive wastes. *J Iber Geol*. 2006;32:7–14.
5. Delage P, Cui Y-J, Tang A. Clays in radioactive waste disposal. *J Rock Mech Geotech Eng*. 2010;2:111–123. http://dx.doi.org/10.3724/SP.J.1235.2010.00111.
6. Chapman N, Hooper A. The disposal of radioactive wastes underground. *Proc Geol Assoc*. 2012;123:46–63. http://dx.doi.org/10.1016/j.pgeola.2011.10.001.
7. Hedin A. *Long-Term Safety for KBS-3 Repositories at Forsmark and Laxemar—A First Evaluation. Main Report of the SR-Can Project*. Svensk Kärnbränslehantering AB (SKB) Tech. Rep. TR-06-09, Stockholm, Sweden: 2006.
8. Liu L. Permeability and expansibility of sodium bentonite in dilute solutions. *Colloids Surf A*. 2010;358(1–3):68–78. http://dx.doi.org/10.1016/j.colsurfa.2010.01.033.
9. Andra. *Référentiel des Matériaux d'un Stockage De Déchets à Haute Activité et à Vie Longue—Tome 4: les Matériaux à Base D'argilites Excavées et Remaniées*. ANDRA Tech. Rep. CRPASCM040015B, France: 2005.
10. Martin PL, Barcala JM, Huertas F. Large-scale and long-term coupled thermo-hydro-mechanic experiments with bentonite: the febex mock-up test. *J Iber Geol*. 2006;32(2):259–282.
11. Juvankoski M. *Description of Basic Design for Buffer (Working Report 2009-131)*. Technical Rep., Eurajoki, Finland; 2010.
12. Wang Q, Tang AM, Cui Y-J, Delage P, Barnichon J-D, Ye WM. The effects of technological voids on the hydro-mechanical behaviour of compacted bentonite–sand mixture. *Soils Found*. 2013;53(2):232–245. http://dx.doi.org/10.1016/j.sandf.2013.02.004.
13. Pusch R. *The Buffer and Backfill Handbook, Part 1: Definitions, Basic Relationships, and Laboratory Methods*. Svensk Kärnbränslehantering AB (SKB) Tech. Rep. TR-02-20, Stockholm, Sweden; 2002.
14. Wersin P, Johnson L, McKinley I. Performance of the bentonite barrier at temperatures beyond 100: A critical review. *Phys Chem Earth*. 2007;32(Parts A/B/C):780–788. http://dx.doi.org/10.1016/j.pce.2006.02.051.
15. Gens A, Valleján B, Zandarín M, Sánchez M. Homogenization in clay barriers and seals: Two case studies. *J Rock Mech Geotech Eng*. 2013;5(Parts A/B/C):191–199. http://dx.doi.org/10.1016/j.jrmge.2013.04.003.
16. Deniau I, Devol-Brown I, Derenne S, Behar F, Largeau C. Comparison of the bulk geochemical features and thermal reactivity of kerogens from mol (boom clay), bure (callovo-oxfordian argillite) and tournemire (toarcian shales) underground research laboratories. *Sci Total Environ*. 2008;389:475–485. http://dx.doi.org/10.1016/j.scitotenv.2007.09.013.
17. Villar MV, Lloret A. Influence of dry density and water content on the swelling of a compacted bentonite. *Appl Clay Sci*. 2008;39(1–2):38–49. http://dx.doi.org/10.1016/j.clay.2007.04.007.
18. Zheng L, Rutqvist J, Birkholzer JT, Liu H-H. On the impact of temperatures up to 200 °C in clay repositories with bentonite engineer barrier systems: A study with coupled thermal, hydrological, chemical, and mechanical modelling. *Eng Geol*. 2015;197:278–295. http://dx.doi.org/10.1016/j.enggeo.2015.08.026.
19. Daniels KA, Harrington JF, Zihms SG, Wiseall AC. Bentonite permeability at elevated temperature. *Geosciences*. 2017;7(3). http://dx.doi.org/10.3390/geosciences7010003.
20. SKB. *Final Storage of Spent Nuclear Fuel—KBS-3*. Stockholm, Sweden: 1983.
21. NAGRA. *Project Gewahr 1985, Nuclear Waste Management in Switzerland: Feasibility Studies and Safety Analysis*. Tech. Rep. NAGRA-NTB-85-09, 1985.
22. Coulon H, Lajudie A, Debrabant P, Atabek R, Jordia M, Jehan RA. Choice of french clays as engineered barrier components for waste disposal. *Sci. Basis Nucl Waste Manag*. 1987;10:813–824. http://dx.doi.org/10.1557/PROC-84-813.
23. Linares J. *Spanish Research Activities in Thefield of Backfilling and Sealing: a Pre-Liminary Study of Some Spanish Sedimentary (Madrid Basin) and Hydrothermal (Almeria) Bentonite*. Proc. of an NEA/CEC Workshop on Sealing of RadioactiveWaste Repositories Tech. Rep., Paris: 1989:318–332.
24. Vieno T, Hautojarvi A, Koskinen L, Nordman H. *TVO-92 Safety Analysis Ofspent Fuel Disposal*. Technical Research Center Tech. Rep. VTJ-92-33E, Finland: 1992.
25. Pusch R. *The Microstructure of MX-80 Clay with Respect to Its Bulk Physical Properties Under Different Environmental Conditions*. Svensk Kärnbränslehantering AB (SKB) Tech. Rep. TR-01-08, Stockholm, Sweden: 2001.
26. Villar M. *Thermo-hydro-mechanical characterisation of a bentonite from Cabo de Gata. A study applied to the use of bentonite as sealing material in high level radioactive waste repositories*. Empresa Nacional de Residuos Radioactivos (ENRESA) Tech. Rep. 01/2002, Madrid, Spain: 2002.
27. Villar MV, Iglesias RJ, García-Sieriz JL. State of the in situ febex test (GTS, Switzerland) after 18 years: a heterogeneous bentonite barrier. *Environ Geotech*. 2020;7(2):147–159. http://dx.doi.org/10.1680/jenge.17.00093.
28. Cui Y. On the hydro-mechanical behaviour of MX80 bentonite-based materials. *J Rock Mech Geotech Eng*. 2017;9(3):565–574. http://dx.doi.org/10.1016/j.jrmge.2016.09.003.
29. Marcial D, Delage P, Cui YJ. On the high stress compression of bentonites. *Can Geotech J*. 2002;39(4):812–820. http://dx.doi.org/10.1139/t02-019.
30. Ben Rhaïem H, Pons C, Tessier D. *Factors Affecting the Microstructure of Smectites. Role of Cations and History of Applied Stresses*. Proceedings of the International Clay Conference, The Clay Mineral Society, Tech. Rep., Denver: 1987:292–297.
31. Thomson S, Ali P. *A Laboratory Study of the Swelling Properties of Sodium and Calcium Modifications of Lake Edmon Clay*. Proc. 2nd Int. Res. and Eng. Conf. Expans. Soils, Tech. Rep., Texas A and M University, USA: 1969:256–262.
32. Westsik J, Bray L, Hodges F, Wheelwright E. Permeability, swelling and radionuclide retardation properties of candidate backfill materials. *Sci Basis Nucl Waste Manag*. 1982. http://dx.doi.org/10.1557/PROC-6-329.
33. Börgesson L, Pusch R. *Rheological Properties of a Calcium Smectite*. Svensk Kärnbränslehantering AB (SKB) Tech. Rep. TR-87-31, Stockholm, Sweden; 1987.
34. Gens A, Alonso E. A framework for the behaviour of unsaturated clay. *Can Geotech J*. 1992;29:1013–1032. http://dx.doi.org/10.1139/t92-120.
35. Delage P, Howat MD, Cui Y-J. The relationship between suction and swelling properties in a heavily compacted unsaturated clay. *Eng Geol*. 1998;50:31–48. http://dx.doi.org/10.1016/S0013-7952(97)00083-5.

36. Cui Y, Yahia-Aissa M, Delage P. A model for the volume change behaviour of heavily compacted swelling clays. *Eng Geol*. 2002;64:233–250. http://dx.doi.org/10.1016/S0013-7952(01)00113-2.
37. Karnland O, Muurinen A, Karlsson F. *Bentonite Swelling Pressure in Nacl Solutions: Experimentally Determined Data and Model Calculations*. Symposium On Large-Scale Field Tests in Granite, Tech. Rep., Sitges, Spain: 2002.
38. Xie M, Moog H, Kolditz O. *Geochemical Effects on Swelling Pressure of Highly Compacted Bentonite: Experiments and Model Analysis*. Theoretical and Numerical Unsaturated Soil Mechanics Tech. Rep., 113, Springer Proceedings in Physics, Berlin/Heidelberg: 2007:93–100.
39. Jönsson B, Kesson T, Jönsson B, Meehdi S, Janiak J, Wallenberg R. *Structure and Forces in Bentonite MX-80*. Svensk Kärnbränslehantering AB (SKB) Tech. Rep. TR-09-06, Stockholm, Sweden: 2009.
40. Lee JO, Lim JG, Kang IM, Kwon S. Swelling pressures of compacted Ca-bentonite. *Eng Geol*. 2012;129–130:20–26. http://dx.doi.org/10.1016/j.enggeo.2012.01.005.
41. Pusch R. *Water Uptake Migration, and Swelling Characteristics of Unsaturated and Saturated Highly Compacted Bentonite*. Svensk Kärnbränslehantering AB (SKB) Tech. Rep. TR-80-11, Stockholm, Sweden: 1980.
42. Pusch R. *Swelling Pressure of Highly Compacted Bentonite*. Svensk Kärnbränslehantering AB (SKB) Tech. Rep. TR-80-13, Stockholm, Sweden: 1980.
43. Gray MN, Cheung SCH, Dixon A. *The Influence of Sand Content on Swelling Pressures and Structure Developed in Statically Compacted Na-Bentonite*. Atomic Energy of Canada Limited Tech. rep. AECL-7825, Canada: 1984.
44. Saba S, Barnichon J, Cui Y, Tang A, Delage P. Microstructure and anisotropic swelling behaviour of compacted bentonite/sand mixture. *J Rock Mech Geotech Eng*. 2014;6(2):126–132. http://dx.doi.org/10.1016/j.jrmge.2014.01.00.
45. Horseman S, Harrington J, Sellin P. *Water and Gas Flow in Mx80 Bentonite Buffer Clay*. Materials Research Society Symposium on the Scientific Basis for Nuclear Waste Management XXVII Tech. Rep., 807, Kalmar: 2004:715–720.
46. Harrington JF, Birchall DJ, Noy DJ, Cuss RJ. *Large Scale Gas Injection Test (Lasgit) Performed at the Äspö Hard Rock Laboratory: Summary Report 2007*. British Geological Survey Tech. Rep. CR-07-211, Nottingham, UK: 2008.
47. Cuss RJ, Harrington JF, Noy DJ. *Large Scale Gas Injection Test (Lasgit) Performed at the Aspo Hard Rock Laboratory: Summary Report 2008*. Svensk Kärnbränslehantering AB (SKB) Tech. Rep. TR-10-38, Stockholm, Sweden: 2010.
48. Harrington JF, Tamayo-Mas E. *Observational Evidence for the Differential Development of Porewater Pressure within Compact Bentonite and its Impact on Permeability and Swelling Pressure*. British Geological Survey Tech. Rep. CR-16-160, Nottingham, UK: 2016.
49. Harrington JF, Daniels KA, Tamayo-Mas E. *Homogenisation on the Laboratory Scale: Development of Porewater Pressure and Stress in Bentonite*. British Geological Survey Tech. Rep. CR-17-142, Nottingham, UK: 2017.
50. Brackley I. *Swell Pressure and Free Swell in Compacted Clay*. Tech. Rep., 3rd International Conference of Expansive Soils. National Building Research Institute, Council for Scientific and Industrial Research, Haifa: 1973:169–176.
51. Gens A, Valleján B, Sánchez M, Imbert C, Villar M, Van Geet M. Hydromechanical behaviour of a heterogeneous compacted soil: experimental observations and modelling. *Géotechnique*. 2011;61:367–386. http://dx.doi.org/10.1680/geot.SIP11.P.015.
52. Imbert C, Villar MV. Hydro-mechanical response of a bentonite pellets/powder mixture upon infiltration. *Appl Clay Sci*. 2006;32:197–209. http://dx.doi.org/10.1016/j.clay.2006.01.005.
53. Pusch R. Mineral–water interactions and their influence on the physical behaviour of highly compacted Na bentonite. *Can Geotech J*. 1982;19:381. http://dx.doi.org/10.1139/t82-041.
54. Schanz T, Tripathy S. Swelling pressure of a divalent-rich bentonite: diffuse double-layer theory revisited. *Water Resour Res*. 2009;45:W00C12. http://dx.doi.org/10.1029/2007WR006495.
55. Massat L, Cuisinier O, Bihannic I, Claret F, Pelletier M, Masrouri F, Gaboreau S. Swelling pressure development and inter-aggregate porosity evolution upon hydration of a compacted swelling clay. *Appl Clay Sci*. 2016;124–125:197–210.
56. NEA-OECD. *Post-Closure Safety Case for Geological Repositories. Nature and Purpose*. Nuclear Energy Agency Technical Rep., 2004.
57. Wigger C, Hanusová I, Hausmannová L, Heino V, Lavikainen L, Leupin OX, Marshall P, Mayor JC, Meleshyn A, Pusch R, Sellin P, Swahn J, Talandier J, Wendling J, Wieczorek K. *Beacon - Bentonite Mechanical Evolution State-of-the-Art Report*. Tech. Rep., 2017.
58. Rabinowicz E. *Friction and Wear of Materials*. New York: John Wiley; 1965.
59. Byerlee JD. The mechanics of stick-slip. *Tectonophysics*. 1970;9:475–486. http://dx.doi.org/10.1016/0040-1951(70)90059-4.
60. Dieterich JH. Time-dependent friction and the mechanics of stick-slip. *Pure Appl Geophys*. 1978;116:790–806. http://dx.doi.org/10.1007/BF00876539.
61. Doanh T, Hoang MT, Roux J, Dequeker C. Stick-slip behaviour of model granular materials in drained triaxial compression. *Granul Matter*. 2013;15:1–23. http://dx.doi.org/10.1007/s10035-012-0384-6.
62. Harrington JF, Graham CC, Cuss RJ, Norris S. Gas network development in a precompacted bentonite experiment: Evidence of generation and evolution. *Appl Clay Sci*. 2017;147:80–89. http://dx.doi.org/10.1016/j.clay.2017.07.005.